NAVAL POSTGRADUATE SCHOOL
Monterey, California

THESIS

MICROTEXTURAL CHARACTERIZATION OF SHEAR TEXTURES IN THE THERMO-MECHANICALLY AFFECTED ZONE OF FRICTION STIR PROCESSED NICKEL ALUMINUM BRONZE

by

Charles Frederick Walton, Jr.

June 2003

Thesis Advisor: Terry R. McNelley

Approved for public release; distribution is unlimited

THIS PAGE INTENTIONALLY LEFT BLANK

REPORT DOCUMENTATION PAGE			Form Approved OMB No. 0704-0188
Public reporting burden for this collection of information is estimated to average 1 hour per response, including the time for reviewing instruction, searching existing data sources, gathering and maintaining the data needed, and completing and reviewing the collection of information. Send comments regarding this burden estimate or any other aspect of this collection of information, including suggestions for reducing this burden, to Washington headquarters Services, Directorate for Information Operations and Reports, 1215 Jefferson Davis Highway, Suite 1204, Arlington, VA 22202-4302, and to the Office of Management and Budget, Paperwork Reduction Project (0704-0188) Washington DC 20503.			
1. AGENCY USE ONLY *(Leave blank)*	**2. REPORT DATE** June 2003	**3. REPORT TYPE AND DATES COVERED** Master's Thesis	
4. TITLE AND SUBTITLE: Microtextural Characterization of Shear Textures in the Thermo-mechanically Affected Zone of Friction Stir Processed Nickel Aluminum Bronze.			**5. FUNDING NUMBERS**
6. AUTHOR(S) Walton, Jr. Charles F.			
7. PERFORMING ORGANIZATION NAME(S) AND ADDRESS(ES) Naval Postgraduate School Monterey, CA 93943-5000			**8. PERFORMING ORGANIZATION REPORT NUMBER**
9. SPONSORING /MONITORING AGENCY NAME(S) AND ADDRESS(ES) N/A			**10. SPONSORING/MONITORING AGENCY REPORT NUMBER**
11. SUPPLEMENTARY NOTES The views expressed in this thesis are those of the author and do not reflect the official policy or position of the Department of Defense or the U.S. Government.			
12a. DISTRIBUTION / AVAILABILITY STATEMENT Approved for public release; distribution is unlimited			**12b. DISTRIBUTION CODE**

13. ABSTRACT ***(maximum 200 words)*** Cast nickel-aluminum bronze (NAB) is used in the production of the Navy's marine propellers for both surface and submersible platforms. Improving the properties of NAB will facilitate new designs. Friction Stir Processing (FSP) is a solid state, thermo-mechanical process to achieved surface hardening of cast NAB by use of a rotating tool that is plunged into and traversed across the material surface. The subsequent "stirring" action produces local yielding/softening of the material by frictional as well as adiabatic heating. The softened regions experience extensive shear deformations resulting in refinement and homogenization of the local microstructure. In essence, FSP can be used to achieve a wrought microstructure from as-cast nickel-aluminum bronze in the absence of macroscopic shape change. There is a region known as the Thermo-mechanically Affected Zone, or TMAZ, in material that has experienced FSP. This region, similar to the heat affected zone (HAZ) common in fusion welding, displays a microstructure characteristic of one affected by diffusion of heat, as well as deformation induced by the rotating tool resulting in the development of shear textures. Using Orientation Imaging Microscopy (OIM) these shear textures were analyzed and characterized for two separate FSP conditions. Through OIM, shear textures in the TMAZ were characterized to be of the C-type, with varied lattice orientations. Shear directions were predominately in the direction of tool advance for one processing condition, while tangent to the tool interface for the other.

14. SUBJECT TERMS Nickel Aluminum Bronze, Friction Stir Processing, Orientation Imaging Microscopy, Optical Microscopy, Thermo-mechanically Affected Zone, Shear Plane, Shear Deformation, Shear Texture			**15. NUMBER OF PAGES 75**
			16. PRICE CODE
17. SECURITY CLASSIFICATION OF REPORT Unclassified	**18. SECURITY CLASSIFICATION OF THIS PAGE** Unclassified	**19. SECURITY CLASSIFICATION OF ABSTRACT** Unclassified	**20. LIMITATION OF ABSTRACT** UL

NSN 7540-01-280-5500 Standard Form 298 (Rev. 2-89)
Prescribed by ANSI Std. 239-18

THIS PAGE INTENTIONALLY LEFT BLANK

Approved for public release; distribution is unlimited

MICROTEXTURAL CHARACTERIZATION OF SHEAR TEXTURES IN THE THERMO-MECHANICALLY AFFECTED ZONE OF FRICTION STIR PROCESSED NICKEL ALUMINUM BRONZE

Charles F. Walton, Jr.
Ensign, United States Navy
B.S. Mechanical Engineering, United States Naval Academy, 2002

Submitted in partial fulfillment of the
requirements for the degree of

MASTER OF SCIENCE IN MECHANICAL ENGINEERING

from the

NAVAL POSTGRADUATE SCHOOL
June 2003

Author: Charles F. Walton, Jr.

Approved by: Terry R. McNelley
Thesis Advisor

Young W. Kwon
Chairman, Department of Mechanical Engineering

THIS PAGE INTENTIONALLY LEFT BLANK

ABSTRACT

Cast nickel-aluminum bronze (NAB) is used in the production of the Navy's marine propellers for both surface and submersible platforms. Improving the properties of NAB will facilitate new designs. Friction Stir Processing (FSP) is a solid state, thermo-mechanical process to achieved surface hardening of cast NAB by use of a rotating tool that is plunged into and traversed across the material surface. The subsequent "stirring" action produces local yielding/softening of the material by frictional as well as adiabatic heating. The softened regions experience extensive shear deformations resulting in refinement and homogenization of the local microstructure. In essence, FSP can be used to achieve a wrought microstructure from as-cast nickel-aluminum bronze in the absence of macroscopic shape change. There is a region known as the Thermo-mechanically Affected Zone, or TMAZ, in material that has experienced FSP. This region, similar to the heat affected zone (HAZ) common in fusion welding, displays a microstructure characteristic of one affected by diffusion of heat, as well as deformation induced by the rotating tool resulting in the development of shear textures. Using Orientation Imaging Microscopy (OIM) these shear textures were analyzed and characterized for two separate FSP conditions. Through OIM, shear textures in the TMAZ were characterized to be of the C-type, with varied lattice orientations. Shear directions were predominately in the direction of tool advance for one processing condition, while tangent to the tool interface for the other.

THIS PAGE INTENTIONALLY LEFT BLANK

TABLE OF CONTENTS

THIS PAGE INTENTIONALLY LEFT BLANK

LIST OF FIGURES

LIST OF TABLES

THIS PAGE INTENTIONALLY LEFT BLANK

LIST OF ABBREVIATIONS, ACRONYMS, AND SYMBOLS

ASTM	American Society for Testing and Materials
BCC	Body Centered Cubic
DRV	Dynamic Recovery
EBSP	Electron Backscatter Pattern
FCC	Face Centered Cubic
FSP	Friction Stir Processing/Processed
HAZ	Heat-Affected Zone
KV	kilovolt
NAB	Nickel Aluminum Bronze
NSWCCD	Naval Surface Warfare Center, Caderock Division
OIM	Orientation Imaging Microscopy
OM	Optical Microscopy
RSC	Rockwell Science Center
SEM	Scanning Electron Microscope
TEM	Transmission Electron Microscope
TMAZ	Thermomechanically-Affected Zone
TWI	The Welding Institute
UNS	Unified Numbering System
Wt. %	Weight Percent
a	alpha
b	beta
k	kappa
g	gamma

THIS PAGE INTENTIONALLY LEFT BLANK

ACKNOWLEDGMENTS

The author would like to express his appreciation to the Defense Advanced Research Projects Agency (DARPA) for their funding and support of this research; the Naval Surface Warfare Center (Caderock Division) for their material and technical support; and, Murray W. Mahoney, Rockwell Science Center for his enthusiasm and endless support.

The author would additionally like to thank Professor Terry McNelley for his guidance throughout the course of this research project.

The author would also like to thank Dr. Keiichiro Oishi, Dr. C. Park and Charles Roe for their assistance in sample preparation as well as in the data collection and technical support for this project.

The author would like to acknowledge William A. Nabach and Kenneth B. Faires for their indefatigable effort and help on this and other related FSP related projects.

The author would like to thank his friends for their humor and unwavering patience.

Finally the author would like to thank his parents and for their love and support throughout this endeavor. Without you this would not have been possible.

THIS PAGE INTENTIONALLY LEFT BLANK

I. INTRODUCTION

A. NICKEL-ALUMINUM BRONZE

Nickel-aluminum bronze (NAB) is a copper based alloy with iron, nickel and aluminum additions that is used extensively for marine applications such as propellers for United States Navy surface and sub-surface platforms because it exhibits excellent corrosion resistance as well as good strength. In addition to its overall strength and corrosion resistance, NAB also demonstrates other important characteristics. These include [Ref. 1] i) good wearabiltiy and low friction coefficients; ii) high damping capacity; iii) exceptional fatigue resistance; iv) good fracture toughness at both elevated and lower temperatures; and v) moderate tensile strength through a wide temperature range. Therefore, the use of NAB is not limited to propeller application; valve parts, fittings, pumps, etc. for both freshwater and seawater service are also fabricated from NAB.

The Navy casts propellers using a NAB alloy designated UNS C95800, commonly referred to as alpha nickel aluminum bronze or propeller bronze [Ref. 2]. NAB propellers are sand-cast in accordance with the ASTM B148 specification for aluminum bronze castings [Ref. 3]. The procedures designated by the ASTM B148 specification give a complicated microstructure [Ref. 4]. Because cooling rates in large castings are nearly impossible to control, varied cooling rates also give rise to non-uniform NAB microstructures and reduced material properties and performance. In addition, gas evolution during solidification and cooling results in porosity, further degrading material strength and corrosion resistance. [Ref 5]

With respect to propellers, the coarse microstructure and porosity developed in casting contribute to an overall reduction in material performance. It is necessary that casting methods of propellers produce the best possible quality of microstructure since a high strength is needed to withstand the forces on the propeller as it engages the water. In addition, weaker microstructures inherent in cast propellers show greater susceptibility to corrosion and fatigue, especially in an aggressive environment such as seawater. [Ref. 6] This, as well as, cavitation due to propeller motion through the water, greatly reduces

the service life. A surface hardening technique that strengthens surface layers of the propeller by improving microstructure and by the removal of casting defects would help resolve many of these difficulties.

Techniques to control and repair defects in cast NAB propellers include welding, which produces a non-equilibrium microstructures and introduces thermal stresses that further degrade corrosion resistance of the alloy. To combat this annealing is used on welded sections, but this yields only a marginal improvement. [Ref. 7] The best circumstance would be a process that creates a fine microstructure in the surface layers while maintaining the ductility of the material. This will ultimately lead to propellers with higher strength and increased cavitation resistance. Friction-stir processing represents the technology required to obtain the aforementioned attributes.

B. FRICTION STIR PROCESSING

FSP is a microstructural refinement process adapted from friction-stir welding [Ref. 8]. The technique uses a rotating tool that is pressed onto and traversed across the material surface to produce extreme plastic deformation as the tool "stirs" the material underneath it. The localized, severe plastic deformation and heating of the material homogenizes the microstructure and thereby improves material properties. The FSP tool consists of a cylindrical "shoulder" with a pin projection at its end that is in contact with the material as it is being processed. The shoulder interacts with the surface of the processed material to forge material softened by the intense deformation and adiabatic heating produced during FSP. What remains is a region of intense shear deformation with a fine-grained microstructure.

It is important to note that, although the intense plastic deformation may transfer material from one side of the tool to the other, FSP is a solid-state process, never melting the processed material. Studies on the effects of friction-stir processing on NAB as well as aluminum and magnesium alloys [Ref. 9-11] reveal that FSP improves material strength as well as ductility, which is desired for propeller application. A direct possibility for this process is not only to repair casting defects, but could radically influence future propeller design. However, a more thorough study of shear textures created in NAB by friction-stir processing is needed.

C. OBJECTIVE OF THIS RESEARCH

The main objective of this research was to characterize and analyze the shear textures that develop in the TMAZ of friction stir processed nickel-aluminum bronze. The TMAZ is a region of a FSP'ed material which experiences mainly heating but also significant plastic deformations. The TMAZ represents an area similar to a heat-affected zone (HAZ) in fusion welding. The motivation for this research is to provide data on shear textures in support of efforts to model or simulate FSP. Analysis of the shear textures is useful because these textures are related to the lattice rotation during deformation of the material. Through lattice orientation data it is possible in turn to infer the local state of stress and strain in the material.

The analysis of shear textures was accomplished using Orientation Imaging Microscopy (OIM). OIM can examine multiple phases within a material as well as yield crystallographic orientation data. This technique was applied to the TMAZ because it has been previously demonstrated that the TMAZ embodies an area where the emergence of shear textures is seen. This research was carried out in order to contribute to the development of a more complete picture of the effect of FSP on NAB, leading to practical application when the process is more fully understood.

THIS PAGE INTENTIONALLY LEFT BLANK

II. BACKGROUND

The composition and phase transformations of NAB will be reviewed in this Chapter. Also, a more in-depth explanation of FSP concentrating on the development of shear through plastic deformation will be considered. In addition, the chapter will attest to the incomparable effects of FSP on NAB microstructure, as well as discuss how known shear textures developed in NAB compare with those developed in other commercial alloys such as aluminum and magnesium alloys.

A. DEVELOPMENT OF NICKEL ALUMINUM BRONZE

Nickel-aluminum bronze is a quaternary alloy based on the Cu-Al system. Composition ranges, including the specific composition used in this research can be found in Table 2.1. Cu-Al binary alloys exhibit the following phases and behaviors: 1) alloys containing less than 7% aluminum solidify as a single-phase α solid solution, with a face-centered cubic (FCC) crystal structure and, upon cooling to room temperature, retain this α phase; 2) alloys with greater than 9.4 wt.% Al solidify as a single-phase β solid solution, which has a body centered cubic (BCC) crystal structure. Upon slow cooling, this β phase forms the α phase, and remnant β transforms by a eutectoid reaction into $\alpha + \gamma$. The Al-rich γ phase has a lower electrochemical potential than the Cu rich α phase. This results in the preferential corrosion or de-aluminization of the alloy. [Ref. 6] Alloying may be employed with Cu-Al alloys to retard the formation of γ.

The additions of nickel and iron into the Cu-Al alloy system effectively extend the α phase while precluding the formation of the γ phase even as the Al content is increased [Ref. 6, 12]. This may be seen in the three ternary equilibrium phase diagrams, for a nominal temperature of 500ºC, which are shown in Figure 2.1. The Ni and Fe additions result in the formation of intermetallic κ phases that replace the γ, and also confer improved material properties in NAB.

	Cu	Al	Ni	Fe	Mn	Si	Pb
min-max	(min) 79.0	8.5-9.5	4.0-5.0	3.5-4.5	0.8-1.5	(max) 0.10	(max) 0.03
Nominal	81	9	5	4	1	-	-
Alloy	81.2	9.39	4.29	3.67	1.20	0.05	<0.005

Table 2.1: Composition (wt.%) of UNS C95800 NAB Material (Metals Hnbk, 9th Ed.) Bottom row represents composition of alloy used in this study.

Alloys containing more than 3 wt. % Fe display a reduction in elevated temperature grain growth in addition to a reduced grain size and a reduced solidification range. [Ref. 12] Higher Fe content (3 - 5 wt. %) increases strength and the retention of this strength at higher temperatures. [Ref. 12] A nominal 4 wt. % Fe has been commonly accepted as the optimum Fe content, greatly improving wear resistance, abrasion resistance, and fatigue endurance. [Ref. 12]

The addition of Ni (0-5 wt.%) increases strength and provides a grain refining effect like Fe. [Ref. 12] The Ni also impedes the formation of the b phase upon cooling and increases hardness. However, it is important to note that alloys with a nickel content less than that of iron are susceptible to second-phase corrosion attack in seawater. A nominal content of 5 wt. % Ni and 4wt. % Fe is deemed ideal for maximum corrosion resistance.

As previously mentioned, the additions of Ni and Fe in nickel-aluminum bronze allow for an increased aluminum content. It has been determined that Al content ranging from 8.8 – 10 wt. % results in good corrosion resistance with increased hardness and strength. [Ref. 12] However, further increases in Al content also results in a decrease in elongation due to increased formation of the lamellar k_{iii} phase, which resides along the grain boundaries. [Ref. 12] The optimum combination of properties appears to be achieved using an Al content of 9.5 wt. % (Table 2.1). The material of this research conforms to the composition limits for NAB.

B. PHASES IN CAST NICKEL ALUMINUM BRONZE

For a nominal 9 wt. % Al content as-cast nickel-aluminum bronze first solidifies as BCC β, as for binary Cu-Al alloys. Upon further cooling the β decomposes to give the four distinct phases of NAB: an FCC α matrix and three κ phases designated κ_{ii}, κ_{iii}, and κ_{iv}. These κ phases have been classified according to both their individual morphologies as observed through optical microscopy (OM) and on the sequence in which they form from the β phase. [Refs 13-14] The phases will be described in this order. These phases are also identified on the micrograph of as-cast NAB shown in Figure 2.2a.

1. Kappa II (κ_{ii})

Originally there were four κ phases classified in as-cast NAB. [Ref. 13] This included a κ_i phase, as well as, the κ_{ii}, κ_{iii}, and κ_{iv} phases. The κ_i phase was of the same composition and crystal structure as the κ_{ii}, only larger in size, and found in alloys containing more that 5 wt. % Fe. The κ_{ii} phase is a globular, dendritic (rosette-shaped) phase in NAB alloys. [Refs 15-16] It can range in particle size from 5 to 50 μm and is iron rich with a nominal Fe_3Al composition. It has been determined that the κ_{ii} phase has a DO_3 crystal structure with a lattice parameter, a, equaling 5.71Å. [Ref 15] The DO_3 structure is defined as an ordered bcc superlattice consisting of eight cells (Figure 2.2b). The first to form from the β phase during cooling, κ_{ii} resides in the center of α grains or in the lamellar eutectoid region of the microstructure. A Cu-Al phase diagram for 5 wt.% Ni and 4 wt. % Fe is represented in Figure 2.3.

2. Alpha (α)

The α phase is an equilibrium solid solution with a face centered cubic (fcc) crystal structure. It has a lattice parameter a= 3.64 Å. [Ref. 15] Alpha forms beginning at about 950^{o}C from β and often displays as a Widmanstätten morphology. This is due to slow cooling from the β phase, which is congruent with the casting of large parts such as propellers. The α can occur intergranularly or intragranularly but slower cooled NAB consists of primarily intragranular α. [Ref. 16] The α phase can be seen as the light phase in figure 2.2a.

3. Kappa IV (k_{iv})

Kappa IV is a fine cuboidal, cruciform precipitate, typically 2 µm in size, formed within the a matrix at 950°C. The k_{iv} particles are of the same Fe_3Al composition and DO_3 crystal structure as the k_{ii} phase. The lattice parameter (a) for the k_{iv} phase is 5.77 Å versus the 5.71 Å for k_{ii}. [Ref. 15]

4. Kappa III (k_{iii})

The k_{iii} phase forms fine lamellar particles following the eutectoid decomposition of b and has a nominal NiAl composition; k_{iii} has a B2 crystal structure with a lattice parameter, a= 2.88 angstroms (approximately half that of k_{ii} and k_{iv}). [Ref. 15, 17] The B_2 structure for NiAl is an ordered CsCl crystal structure, which is hypothesized as forming from k_{ii} particles that may act as a substrate for k_{iii} growth [Ref 17]. Forming at around 800°C, k_{iii} can have a fine lamellar morphology while proeutectoid k_{iii} has a fine, globular morphology.

The casting response of NAB is variable, resulting in varied phase distributions and material properties within the casting. One reason for this is the slow cooling rates inherent in the casting of large structures (i.e. propellers). The other is difficulty in control of alloying composition in NAB. Casting porosity gives further degradation of material properties. This will ultimately lead to lower material strength and decreased cavitation and corrosion resistances.

Propellers experience severe environmental conditions and stresses throughout their service lives. Cavitation, corrosion, and stresses from routine operation serve to erode, corrode and weaken propeller surfaces. Therefore the major concern for manufacturing propellers and larger NAB components is to eliminate the inherent defects in casting without significantly altering the fabrication process. This will extend the service life of the parts and reduce overall maintenance costs. Friction-stir processing, which has been shown to drastically improve the material properties of NAB, can accomplish this task.

C. FRICTION STIR PROCESSING

In 1991 The Welding Institute (TWI) developed a new state of the art welding process known as friction-stir welding (FSW) [Ref. 8]. Friction-stir processing (FSP) represents a groundbreaking microstructural refinement process engendered by FSW technology. Instead of joining two materials as in friction-stir welding FSP processes one material through the use of a "stirring" motion, which, in turn, homogenizes and improves material microstructure.

Friction-stir processing uses a non-consumable tool attached to a modified milling machine. The tool, often fabricated of tool steel, consists of a cylindrical shoulder with a smaller diameter concentric pin at its end. The tool is rotated and plunged into the clamped material (to avoid excessive movement) until the shoulder engages the material surface, as seen in the schematic of Figure 2.4. Once engaged the tool is then traversed across the material surface in a single pass or in multiple passes. The shoulder and length of the pin control the depth of surface penetration. The rotating pin, through mainly sticking friction (there is also some sliding friction), induces plastic deformation and adiabatic heating on a small column of material near the tool center. A larger region of material around the central column is plastically deformed by contact with the rotating shoulder. The shoulder also acts to contain the upward flow of metal that is being physically displaced by the pin, and to forge heated material. Tool shoulder diameter is typically approximately 25 mm, with pin diameter generally between 6 and 10 mm and pin depth ranging from 6 to 12 mm. [Ref. 18] The sticking friction and large plastic deformations produce adiabatic heating of the material. This heating softens the material but does not melt it. A typical temperature distribution calculated for FSP is seen in Figure 2.5. Friction-stir processing is a solid-state process, with the intense plasticity of FSP moving material from one side of the tool and depositing it on the other. Once completed, a processed NAB sample consists of three distinct regions, namely the 1) stir zone/ nugget, 2) the thermo-mechanically affected zone, 3) base metal (Figure 2.6).

The stir zone, or nugget, is the region most highly affected by FSP. It is characterized by intense plastic deformation and a resultant fine-grained, defect free microstructure. The nugget represents the objective of friction-stir processing: a refined

microstructure with improved material properties. Grain sizes in the stir zone are refined to perhaps 3 μm. [Ref. 7] Tensile tests of specimens fabricated from the stir zone of NAB revealed a doubling of yield strength coupled with an approximate 66% increase in ultimate tensile strength. (Figure 2.7a) A significant increase in ductility was observed as well. The stir zone and TMAZ exhibit increased hardness compared to base metal as well. (Figure 2.7b) The stir zone in nickel-aluminum bronze may be heterogeneous, comprised of fine, equiaxed grains in some regions as well as Widmenstätten structures elsewhere. Beneath the stir zone is a region of less severe plastic deformation and heating effects, identified as the thermo-mechanically affected zone (TMAZ).

The TMAZ exhibits some similarity to a heat-affected zone (HAZ) in conventional fusion welding, and represents the focus of this research. This region is characterized by large plastic deformations (but not as much as the stir zone) coupled with heating effects created by adiabatic heating due to the rotating tool. Therefore, the TMAZ experiences steep strain, strain rate and temperature gradients over a distance of approximately 200 to 400 μm. The combination of these effects results in the development of shear textures in the region. What are shear textures? Plastic deformation (as induced in FSP) occurs by shear through the motion of lattice dislocations. The motion of dislocations causes the rotation of the crystal lattice of the material, giving rise to shear textures. In NAB these shear textures are hypothesized as stemming from slip deformation under conditions that give rise to dynamic recovery (DRV), inducing the formation of sub-grains which experience a continuous increase in misorientation. [Ref. 7] Work done on other friction stir processed materials, most notably aluminum and magnesium, indicates shear textures developed that involved alignment of the apparent shear plane with a plane tangent to the TMAZ or tool interface. [Ref. 19-20] The understanding of shear textures is important for it provides insight into the stresses and strains experienced by the metal in this region. Understanding these stresses and strains enables the modeling of this process for individual materials through computer simulation. Previous work suggests that the shear textures developed in the TMAZ of friction-stir processed NAB are of the C type as defined by Canova, et al. [Ref. 21]

The grain structure in the TMAZ consists of larger and distorted grains than in the stir zone. However, it is of note that the TMAZ exhibits improved material properties (and freedom from defects) when compared to the parent material. This is because FSP is a solid-state process. In fusion welding, high temperatures in the weld zone melt the material and subsequent cooling allows extensive grain growth. Both of these phenomena act to degrade the material properties in the HAZ. Conversely, remaining in a solid state means that temperatures in FSP do not reach those associated with melting thereby reducing the degree of grain growth.

The base metal embodies the bulk of the material, which remains relatively unaffected by processing except for minor heating effects near the base metal/ TMAZ interface. Base metal will exhibit a microstructure and material properties dependant upon on the casting conditions. This includes defects.

The microstructure of friction-stir processed NAB is not uniform. Grain size varies throughout the stir zone and TMAZ. This may be attributed to many factors including tool rotation speed and translation rate leading to varying peak temperatures and times at these temperatures [Ref 7]. However, although varied, all processed microstructures exhibit material properties superior to those of parent metal. Friction-stir processed NAB is devoid of porosity.

FSP can produce localized microstructural changes, enabling the freedom to process only selected areas of a material. Processing creates very little noise and is non-toxic, emitting no noxious fumes or gases. In addition, no special material preparation is required prior to processing and the tool is reusable. Because of these attributes, FSP can be performed in numerous environments, is safe, and is inexpensive.

FSP is an important future material processing technology. However before it can be used on a scale beyond experimental, every aspect of the process and its effects on the material require understanding. The motivation for this research derives its basis from this concept. The ability to model or simulate FSP for nickel-aluminum bronze is a viable undertaking, but requires extensive experimentation and patience.

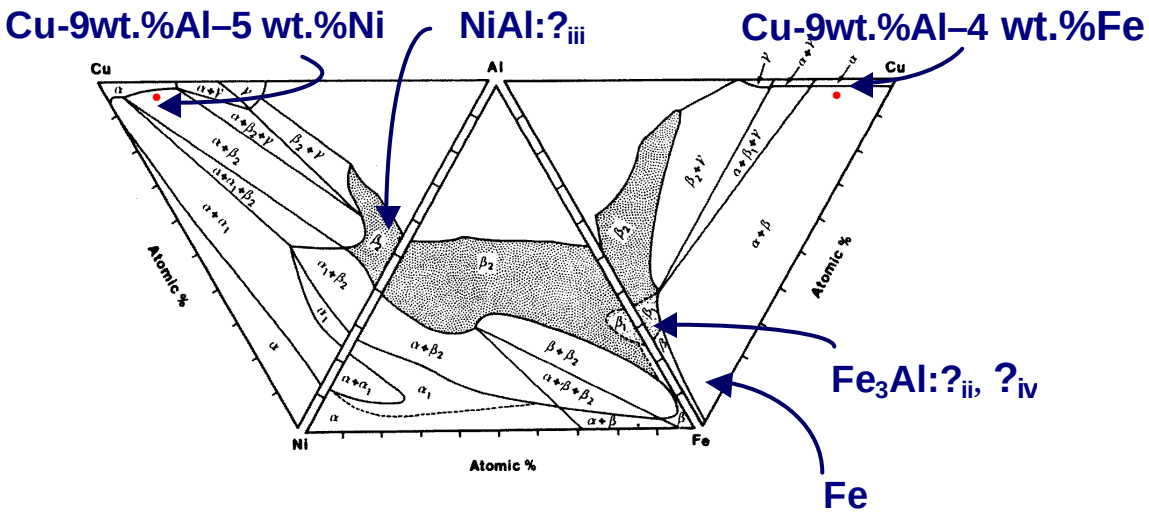

Figure 2.1: Ternary equilibrium phase diagrams for NAB at 500°C. [Modified from Ref. 15]

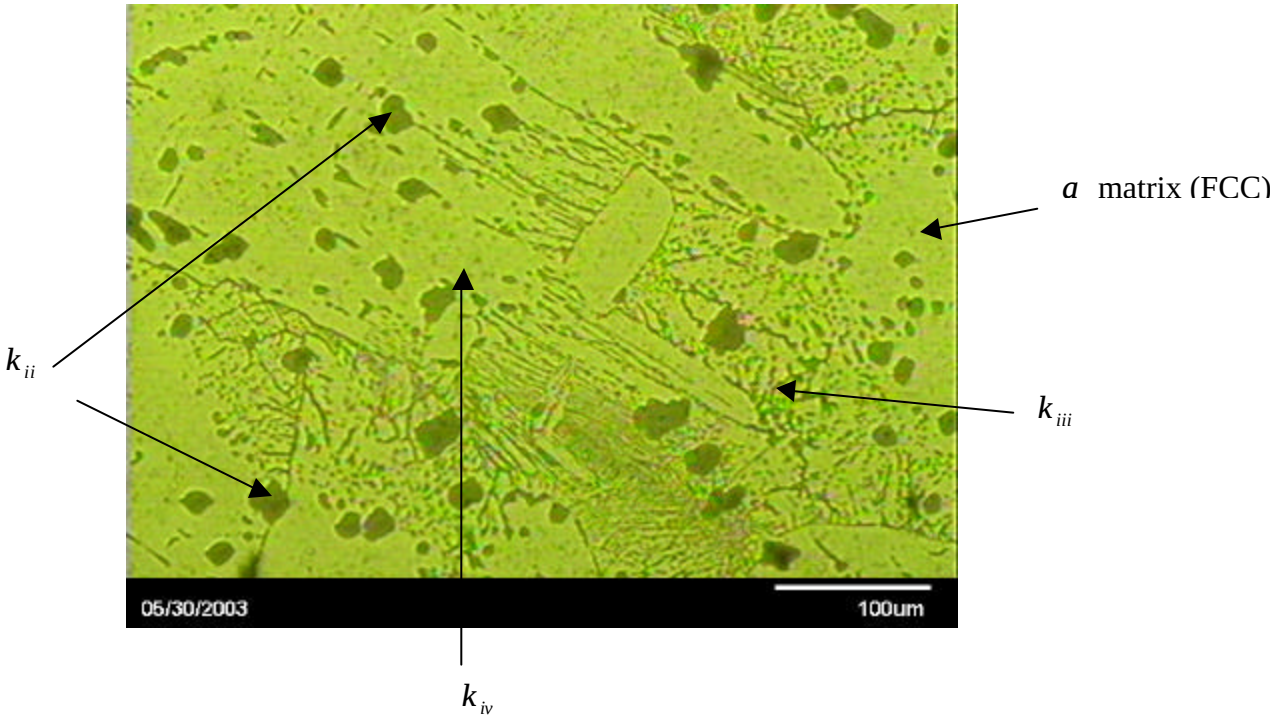

Figure 2.2a: Optical micrograph of as-cast NAB at 370x. k_{ii} is the globular, dendritic structure, k_{iv} is the very fine particulate imbedded with in the α matrix (surrounding phase), k_{iii} is the lamellar "finger-like" structure. As polished, no etch [Ref. 22]

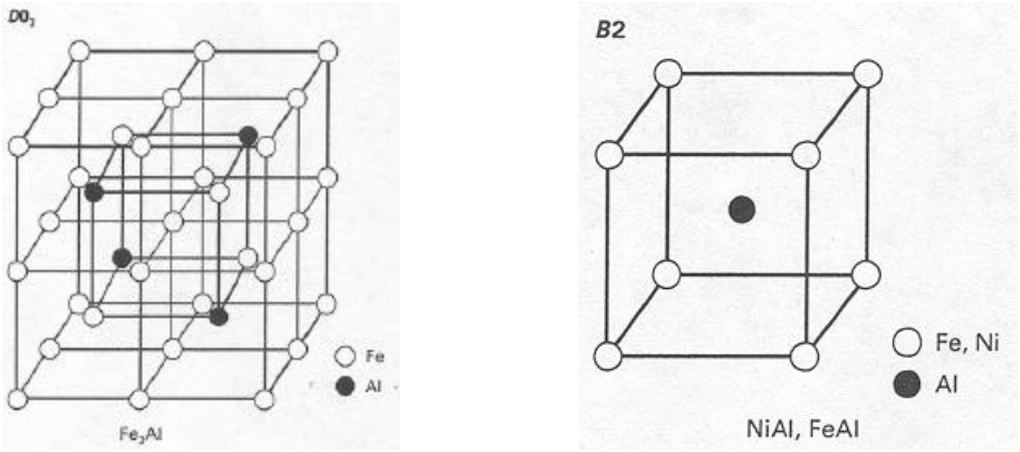

Figure 2.2b: DO_3 and B_2 crystal structures. k_{ii} and k_{iv} have a Fe_3Al compostion with a $D0_3$ crystal structure, while k_{iii} exhibits a NiAl composition with a B_2 crystal structure. [Ref. 23]

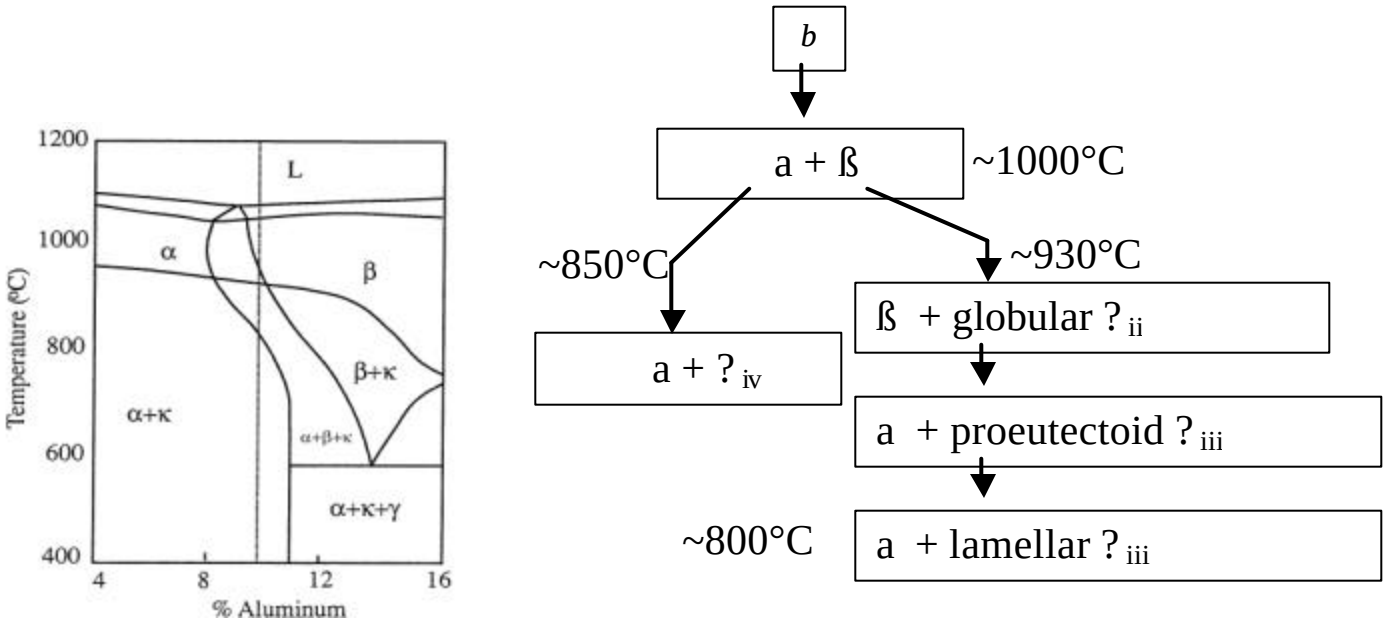

Figure 2.3: NAB phase diagram with corresponding transformation diagram. [Ref 13&21]

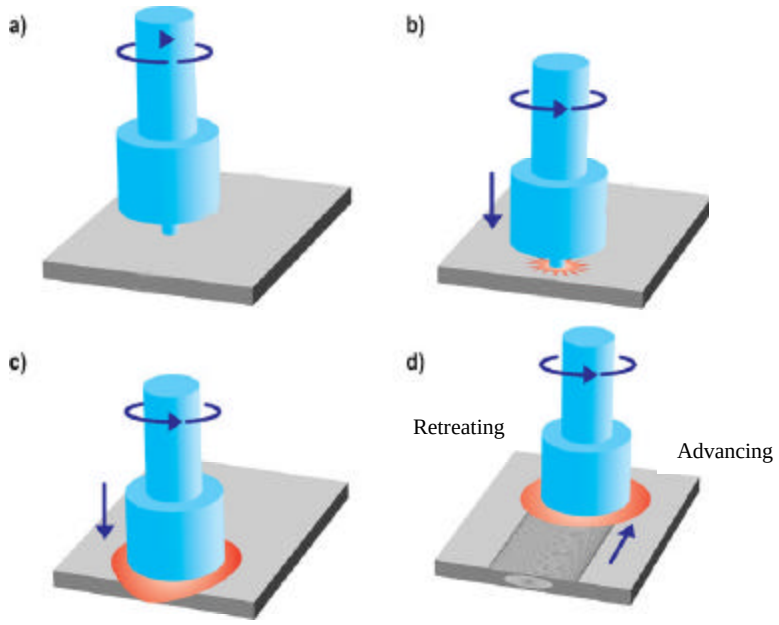

Figure 2.4: Friction Stir Process. A rotating tool a) is plunged into the material surface b). Once engaged up to the shoulder c) the tool is traversed across the material surface d). FSP is not a superficial process, affecting material well below the pin depth. The advancing side is that in which tool rotation and tool translation are in the same direction. On the retreating side tool rotation is opposite tool translation. [Ref. 18]

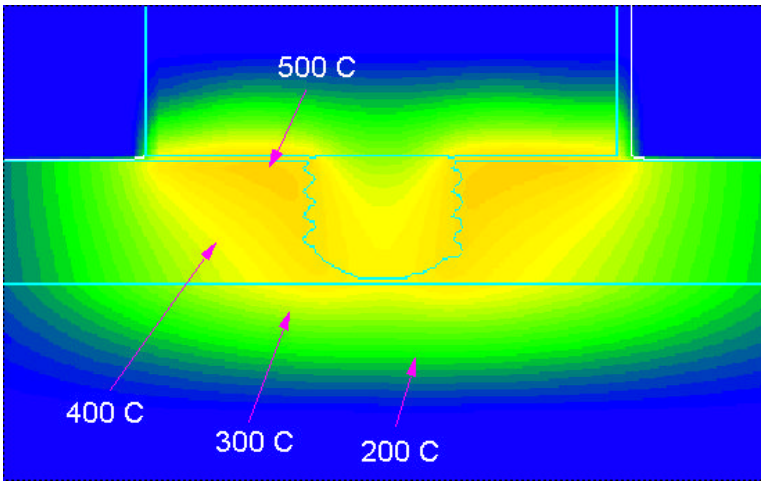

Figure 2.5: Typical results in the modeling of temperature distribution in FSP. Temperatures may reach upwards of 850°C. [Ref. 24]

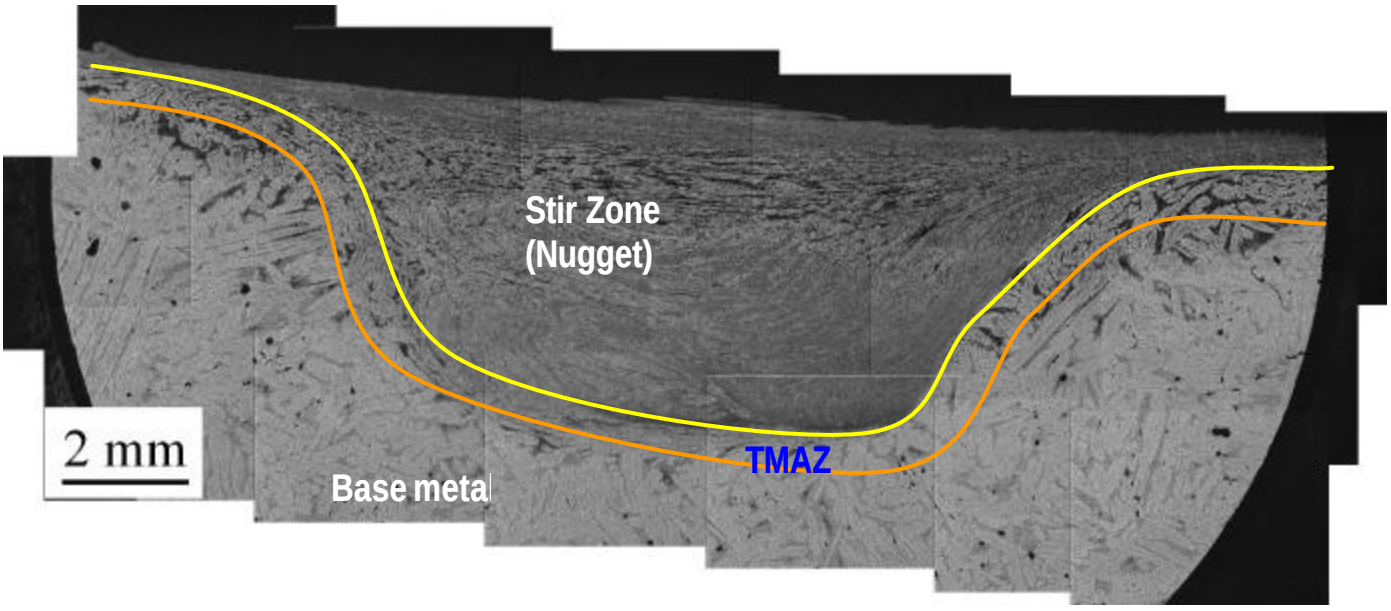

Figure 2.6: Regions resulting from FSP. The stir zone is characterized by extensive plastic deformation as induced by the rotating tool. The TMAZ experiences both large plastic deformations and heating effects. Base metal remains relatively unchanged from the as-cast condition, experiencing minute deformations and heating effects. [Ref. 25]

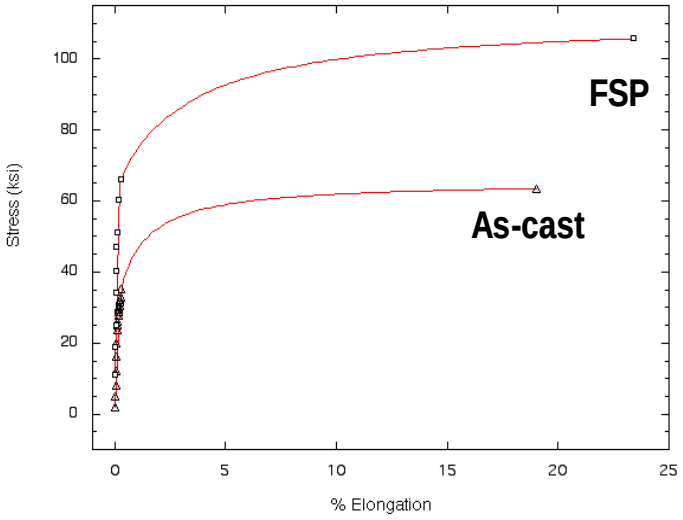

	Yield Strength (ksi)	Tensile Strength (ksi)
FSP	62.8	107.8
As-cast	31.2	64.8

Figure 2.7a: Stress vs strain plot for FSP vs as-cast NAB tensile samples [Ref 18]. Note significant increases in tensile and yield strengths, as well as ductility for FSP'd NAB.

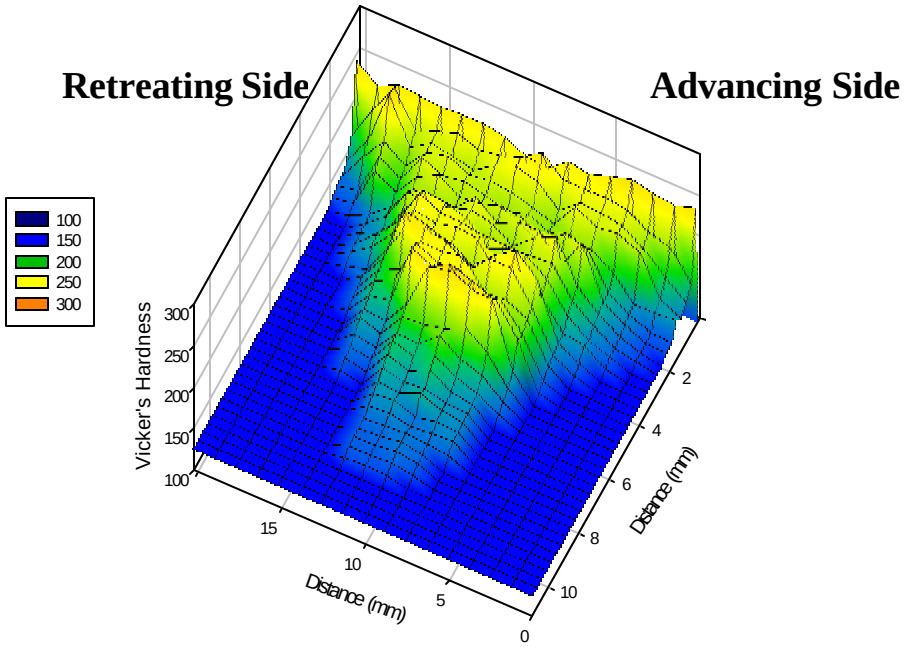

Figure 2.7b: Hardness variation in friction-stir processed NAB. Note large hardness increase in stir zone. [Ref. 26]

THIS PAGE INTENTIONALLY LEFT BLANK

III. EXPERIMENTAL PROCEDURES

A. SAMPLE PREPARATIONS

Rockwell Science Center (RSC), Thousand Oaks, CA, provided two NAB samples that had been subjected to FSP. At RSC processed plates were cut into sections of dimensions 30 mm along a direction transverse to the direction of tool motion, 10 mm along the thickness direction of the processed sample, and 4mm along the direction of tool motion (Figure 3.1) for analysis using OIM. The samples were sectioned in a Buehler saw using a diamond-blade designed to cut medium strength materials. The sections represented two processing conditions, FSP 516 and FSP 520, which are summarized in Table 3.1.

Mechanical polishing of the sectioned samples was accomplished following the polishing schedule outlined in Table 3.2. Steps 1-4 were used to flatten the sample surface in preparation for polishing. Silicon carbide (SiC) paper was used, with distilled water as the lubricant, for these steps. After each step, the sample was rotated 90^{o} until previous abrasions were completely removed. Steps 5-7 were performed, as indicated in Table 3.2, using oil-based diamond suspensions or colloidal silica as polishing mediums. Distilled water was used to add to the lubrication during step 7. Steps 5-7 were conducted for the time specified, rotating the sample 90 degrees approximately every 3 minutes. It is important to note that the times delineated in Table 3.2 are estimates, as the removal of abrasive marks is the most important result. Finally, ultrasonic cleaning was performed for 15 minutes in ethanol after each of steps 5-7 were completed.

Electro-polishing was performed to produce a high quality finish on the samples before analysis using the SEM. This is required due to the small interaction volume of electrons near the surface of the sample during scanning electron microscopy. Electro-polishing for the NAB samples was done at 30V for 10 seconds, using a 33% Nitric Acid-66% Methanol electrolyte solution, cooled to -25^{o}C.

Sample preparation, for a similar study, was conducted at the Rockwell Science Center (RSC) in Thousand Oaks, CA was done in accordance with the schedule outlined in Table 3.2, excluding step 6 (1 μm diamond suspension). Electrolytic etching was

performed using a 25% nitric acid-75% methanol cold solution. The etching voltage was 15V. For optical microscopy, the samples were etched using the following two-step process:

1. Ammonium hydroxide solution: 40% ammonia - 20% hydrogen - 40% water (1-2 seconds)
2. Phosphoric hydroxide solution: 40% phosphoric acid – 10% hydrogen – 60% water (1 second)

For optical microscopy done at the Naval Postgraduate School, the NAB samples were etched according to the RSC process, or with a 10% ammonium persulfate solution.

B. 516/520 FSP SAMPLE PROCESSING

The samples designated FSP 516 and FSP 520 had been processed at RSC using the processing conditions indicated in Table 3.1. The tool used to process both conditions had a shoulder diameter of 23.8mm with a tapered pin 7.95mm in diameter at its base. The pin length also measured 7.95mm. The tool was made of heat-treated tool steel. Samples were always oriented and analyzed in such a way that the direction of tool translation was into the plane of the sample. This means that samples were processed with the advancing side (tool rotation in the same direction as tool translation) on the right and the retreating side (tool rotation opposite tool translation) on the left, indicating that the tool was rotated counter-clockwise as it traversed across the samples.

C. OPTICAL MICROSCOPY

Optical microscopy was performed on the FSP 516 and FSP 520 samples with a Zeiss JENAHPOT 2000 Reflected-Light photomicroscope, equipped with the SEMICAPS Genie SEM digital imaging system.

D. ORIENTATION IMAGING MICROSCOPY (OIM)/ ELECTRON BACKSCATTER PATTERN (EBSP)

Orientation Imaging Microscopy was accomplished using EBSP hardware and software developed by TEXSEM, Inc. These components were installed on a TOPCON SM-510 Scanning Electron Microscope (SEM) using a Tungsten filament operating at an accelerating voltage of 20kV. During analysis the samples were mounted on an SEM holder/stage specifically designed for EBSP/OIM analysis. The holder inclines the sample at 70^{o} to the horizontal so as to orient the sample for EBSP detection.

The SEM was operated in spot mode. A 0.2 μm diameter beam produced by the SEM interacts with the sample bombarding the sample surface with electrons, which undergo Bragg diffraction. These diffracted electrons then impinge on the phosphorous screen of the EBSP detector, illuminating it, and producing a Kikuchi pattern. (Figure 3.2) A low light camera captures this pattern from the screen and sends it to the OIM equipment for analysis.

The OIM software requires that external reference axes be defined to ensure proper analysis. These axes are the reference/rolling direction (RD), the normal direction (ND), and the transverse direction (TD) (figure 3.3a) and are defined as follows:

1. RD: assigned as positive downward along sample surface.
2. ND: assigned as normal to the sample surface toward the phosphor screen.
3. TD: assigned parallel to horizontal along sample surface.

A representation of the sample orientation and system setup is shown in figure 3.3b. In data collection, the OIM software collects various Kikuchi patterns, indexes them, and compares them to similar solutions programmed into the software. A sample Kikuchi pattern and pattern index is displayed in figure 3.4. In practice the software analyses each pattern several times and assigns a matching parameter known as the Confidence Index (CI) by a voting procedure. Thus, a CI of 0.1 corresponds to a 95% probability that the indexed orientation is correct. In addition to the CI, the software will store parameters such as, image quality (IQ) which represents the sharpness or clarity of the observed Kikuchi pattern/data point, Cartesian coordinates of each data point, the indexed phase of each data point, and the Euler angles (which describe lattice orientation) associated with the data point. With this information the software can be manipulated to

produce various figures and representations of the microstructure and its crystallographic orientation. Pole figures, histograms representing the distributions of various quantities, grain orientation maps, cubes representing local lattice orientations, etc. can all be produce using the OIM software. This study focused primarily on the construction and analysis of pole figures in order to determine the shear textures and lattice orientations in the TMAZs of the FSP 516 and FSP 520 samples. The pole figures generated in this study were of the <002>,<022>,and <111> directions for the FCC structure of the α matrix. To produce valuable data, however, the OIM data required "cleaning". Due to various parameters in NAB (i.e., complication of microstructure) some data points are not indexed to a grain. This is usually a result of low CI or IQ associated with the data point. To remedy this, a "clean up" procedure was conducted using the follow steps:

1. Points not belonging to any particular grain are designated to match the neighboring majority grain.
2. Points with CI's below 0.1 are compared to the nearest neighboring grains, and become apart of whichever grain has the largest CI.
3. The highest CI for any grain is assigned to all points in that grain.

Grains exhibiting backscatter patterns of good quality remain unchanged. In addition, any point with a confidence index greater than 0.1 remains unaffected by this "clean up " process.

Scans were conducted using ten 100 μm X 100 μm square areas arranged in two columns and five rows as illustrated in Figure 3.5. The spacing between boxes was limited to 10 μm at most. The step size for each point was set to 1um, creating approximately 11,600 data points for each box. In an effort to explore different mapping techniques the advancing and retreating side corners for the 516 were scanned differently than those of the 520 sample. (Figure 3.5.) The versatility of the OIM software represents its greatest value in micro-structural and micro-textural research.

As previously mentioned, once cleaned, pole figures and grain maps were produced of the FSP 520 and FSP 516 samples in an effort to characterize shear textures

in the material. The results and analysis of this information will be discussed in the subsequent chapter.

	FSP 516	FSP 520
Tool Rotation Speed	800 rpm	1000 rpm
Tool Traversing Rate	6 inch per minute	8 inch per minute
Tool Tilt	3 degrees	3 degrees
Tool shoulder diameter	23.8 mm	23.8 mm

Table 3.1: Processing conditions for Rockwell FSP 516 and FSP 520.

Step	Abrasive	Time	RPM
1	500 Grit SiC Paper	30 sec.	180
2	1000 Grit SiC Paper	30 sec.	180
3	2400 Grit SiC Paper	30 sec.	180
4	4000 Grit SiC Paper	30 sec.	180
5	3 μm Metadi Diamond Suspension	9 min.	80
6	1 μm Metadi Diamond Suspension	9 min.	80
7	0.05 μm Colloidal Silica	15 min.	40

Table 3.2: Mechanical polishing schedule. [Modified from Ref 7.]

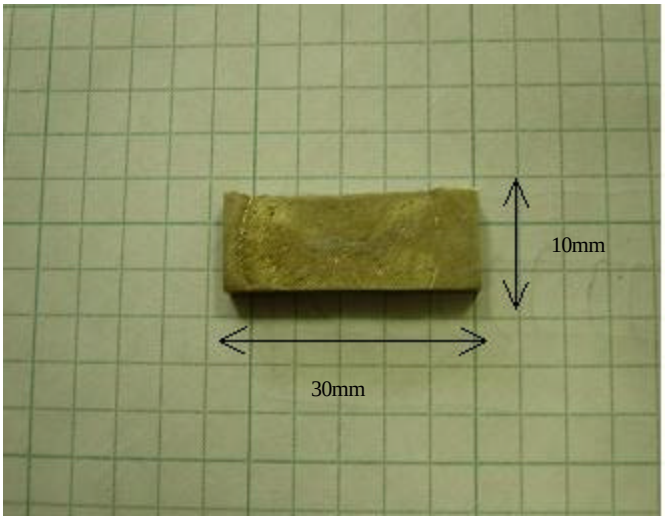

Figure 3.1: Sectioned FSP 516 Sample.

Figure 3.2: Sample Kikuchi Pattern.

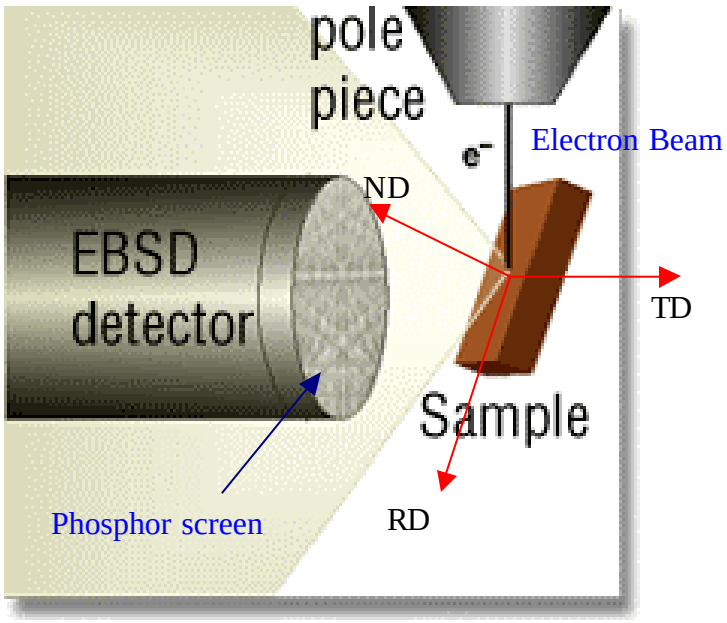

Figure 3.3a: Representative axes for EBSP/OIM coordinate system.

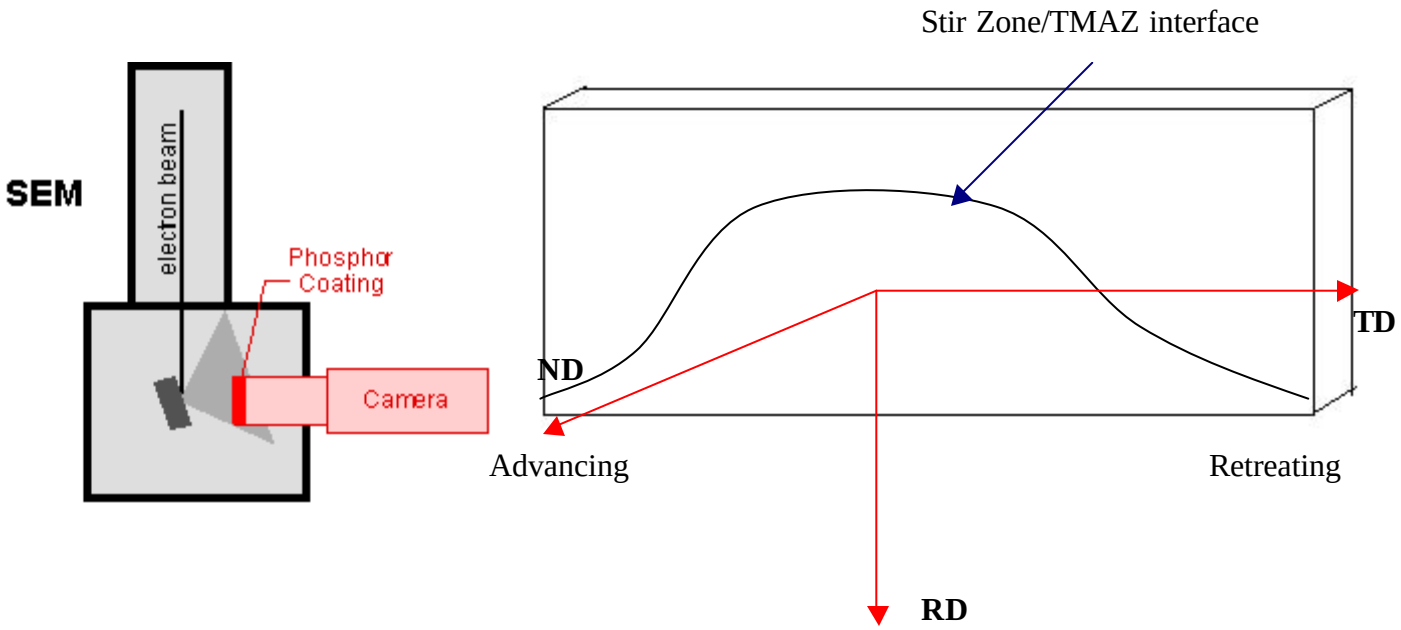

Figure 3.3b: Sketch of actual system and sample orientation used in this research.

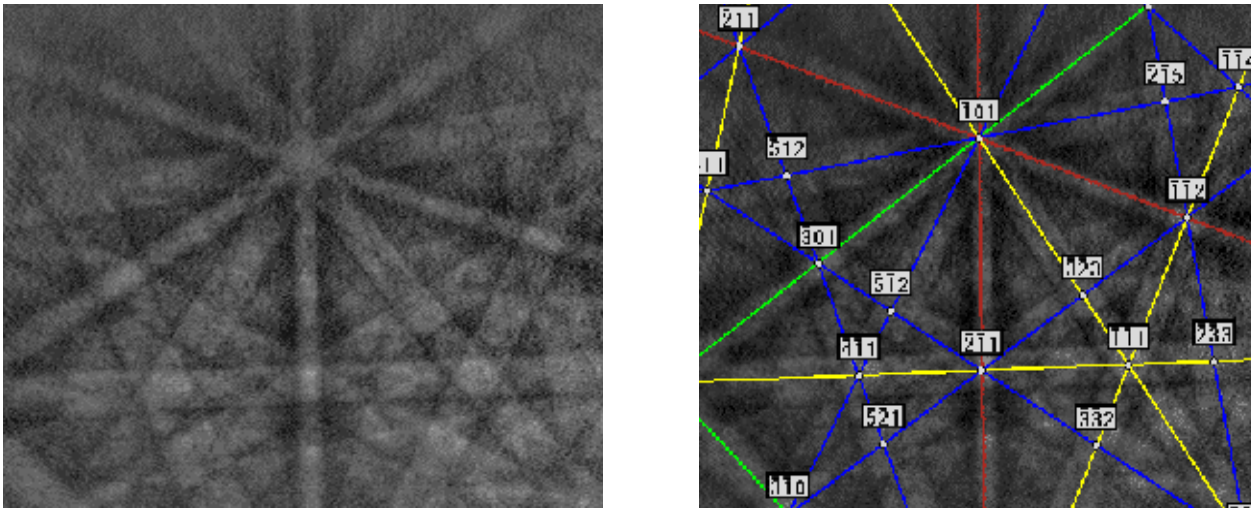

Figure 3.4: Sample Kikuchi pattern and overlaid index.

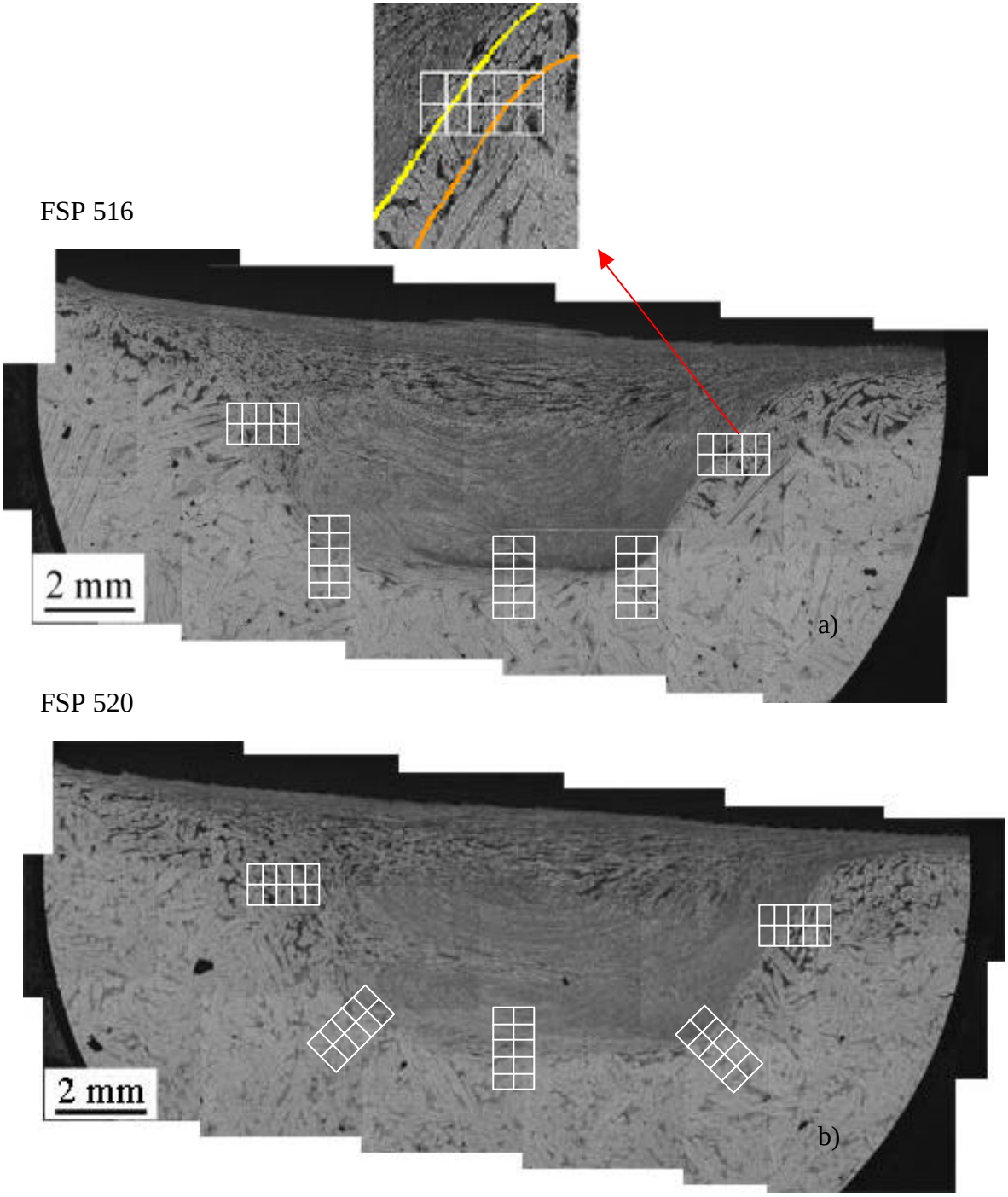

Figure 3.5: Sample Scanning grid and Scanning patterns for a) FSP 516 and b) FSP 520 sample conditions. Each grid square is 100 μm by 100 μm and may be separated by as much as 10 μm. Note that at the retreating and advancing corners scans were completed in a pattern normal to the interface for FSP 520, vice vertical for FSP 516. [Ref. 25]

THIS PAGE INTENTIONALLY LEFT BLANK

IV. RESULTS AND DICUSSION

This chapter will discuss the application of Orientation Imaging Microscopy (OIM) to the analysis of shear textures in the TMAZ in friction stir processed NAB. The shear textures of interest will be those analyzed on the FSP 516 and 520 samples as discussed in the previous chapter. The limitations of OIM in the analysis of these textures and microstructures will also be considered.

A. ORIENTATION IMAGING MICROSCOPY

Orientation imaging microscopy has been used in previous work to identify phases and textures in as-cast NAB and material that had been subjected to FSP. Here, the main focus is on the shear textures in the TMAZ of two NAB materials after FSP. The OIM data collection software [Ref 28] and analysis software [Ref. 29] allow a wide range of data representations, including pole figures and other representations of the texture.

Previous work by Cuevas [Ref. 7] assessed the capability of OIM in analyzing multiphase alloys such as NAB. OIM is an excellent tool for analyzing orientations in single-phase materials. It may also be used for two-phase materials wherein the phases have readily distinguishable crystal structures [Ref. 30-31]. Cuevas [Ref. 7] suggested that OIM is a viable tool for analyzing multiphase alloys such as NAB, although with limitations. The OIM system was able to distinguish the face centered cubic a phase from the various dispersed ? phases but was unable to distinguish among the ? phases because they are ordered cubic structures (i.e., B2 and DO_3 structures) having inter-atom distances that differ by only about one percent. Therefore the current study employed OIM for determination of lattice orientation and shear texture development in the a matrix and the phase discrimination was employed only to distinguish the matrix from the dispersed ? phases.

Cuevas [Ref. 7] documented the presence of shear textures in the TMAZ of an NAB that had been processed by FSP. Canova, Kocks and Jonas [Ref. 21] have described shear textures in terms of an A fiber ({111}<hkl>), a B fiber ({hkl}<110>) and a C

component ({001}<110>), which is located at one end of the B fiber. This notation refers to {plane parallel to the shear plane}<direction parallel to the shear direction>. The shear textures reported by Cuevas [Ref. 7] corresponded closely to the C-type shear texture component. However, the apparent shear plane in the texture often was perpendicular to the interface between the stir zone and the TMAZ. The rotational motion of the tool might suggest that the shear plane would align with the interface. The present work was initiated to obtain further data on two processing conditions in an attempt to clarify the relationship between the texture and FSP conditions.

B. FSP 516

As mentioned previously the FSP 516 sample was processed with a tool rotation rate of 800 revolutions per minute and a traversing speed of 6 inches per minute. The tool used in processing 516 was fabricated from high strength heat-treated tool steel. The tool geometry consisted of a spiral grooved tapered pin with dimensions as delineated in chapter 3. Using OIM, a transverse section of the 516 condition was scanned at five locations (using the procedure and scanning pattern delineated in Chapter 3): 1) the retreating side underneath the shoulder; 2) the retreating side lower corner; 3) the sample center along the bottom of the stir nugget; 4) the advancing side lower corner; 5) the advancing side underneath the shoulder. The following observations are summarized for each of these five locations.

1. Retreating Side Shoulder

As seen in the montage of optical micrographs of Figure 3.5a, the transition from the stir zone is distinct on the advancing side and beneath the tool, but is indistinct on the retreating side, especially in the region of the shoulder where the transition from stir zone into TMAZ is blurred. The TMAZ extends downward at least 2 mm beneath the shoulder before base metal is reached. OIM data confirms that the grain size is fine within the stir zone and coarsens as the transition is made from the stir zone through the TMAZ and toward base metal (see figure 4.1). In the shoulder regions evidence for the formation of a martensitic ß phase is seen in the form of the elongated black regions embedded in the a matrix. (figure 3.5).

In pole figures, each orientation is represented position by set of points on each pole diagram; the number of points depends upon the multiplicity of the set of planes being represented. Preferred orientation is characterized by a grouping of points in the pole figure and, conversely, a random texture, or lack of preferred orientation, as in the stir zone, is indicated by random distribution of points on the pole figures. A random texture is illustrated in Figure 4.2a; this is typical of the stir zones and likely reflects the randomizing effects on orientation of dispersed particles during recrystallization. In contrast, an example of a strong C-type orientation is shown in Figure 4.2b; the trace of the shear plane is approximately aligned with the default RD axis while the shear direction may be either parallel to the RD or aligned with the normal to the diagram.

The TMAZ textures observed at the retreating shoulder in FSP516 were unexpected. From the work of Cuevas [Ref. 7], it was hypothesized that shear textures developing everywhere in the TMAZ would be of a C-type (i.e., orientations near those of Figure 4.2b). Data from the stir zone (Figure 4.3a) are nearly random; in the TMAZ, a near C-type texture component is observed but it is rotated approximately 90º about RD, i.e. about the plate normal, when referred to the sample axes. Further away from the TMAZ the pole figure data still indicate a similar primary orientation but a second, weaker orientation is also apparent that may indicate a grain orientation from base metal. In Al and Mg alloys the observed tendency is for the shear plane to be tangent to the tool / TMAZ interface with the shear direction align with the local direction of tool motion in the shear plane. [Ref.19-20] In consideration of the C-type shear texture component observed here, the crystallographically equivalent combinations of shear plane / shear direction do not align in this fashion with the stir zone / TMAZ interface.

2. Retreating Corner

Figure 4.4 displays scans completed at the retreating corner of the 516 sample. In this region, again, the transition from the stir zone into the TMAZ is somewhat indistinct; however, it is more sharply defined than that at the retreating shoulder location. Almost no martensite is evident in the base metal beyond the TMAZ at this location.

The texture in the TMAZ at the retreating corner (figure 4.4b) coincides with the C-type shear texture. From the (022) pole figure it is noted that a <110> slip (and shear) direction is aligned in the direction of tool advance. However, examination of the crystallographically equivalent combinations of {001}<110> in these data shows that none of them align with the interface between the stir zone / TMAZ interface.

3. Sample Center

Optical microscopy shows a sharp distinction between the stir zone and the TMAZ (figure 3.5), beginning at the center of the sample immediately underneath the direction of tool advance and extending onward to the advancing shoulder location. This distinct transition between regions can be seen on the image quality maps in Figure 4.5 in the form of a rapid change in grain size over a very short distance from the stir zone into base metal.

The TMAZ of the sample center shows a C-type shear texture (Figure 4.5b; compare to Figure 4.2b). In this location, however, it is possible to identify a combination of {001}<110> that align with the stir zone / TMAZ interface. A perspective of a cube representing the lattice orientation in this location is included with the pole figures; examination of this cube reveals that the top and bottom faces ({001} planes) are approximately aligned with this interface. Then, a <110> is aligned approximately with the direction of tool advance and with the transverse direction. Thus, in this location the shear texture is consistent with a local state of shear deformation on a plane parallel to the stir zone / TMAZ interface and in a direction aligned with the tool advance direction, the transverse direction or a combination of these directions. Examination of optical microscopy (Figure 3.5) reveals that the local grain flow pattern in the TMAZ is consistent with such a pattern of shear deformation of the grains at this location.

4. Advancing Corner

The advancing corner exhibits the sharpest delineation between stir zone and TMAZ observed in this sample, as seen in Figure 3.5. Figure 4.6b shows that a C-type shear texture is also prominent in the TMAZ in this location, and a shear direction <110>

may be aligned in the direction of tool advance. Comparison of Figures 4.4b and 4.6b reveals a symmetric relationship of the textures for the retreating and advancing corner locations in that the lattice orientation may be reflected through a plane defined by the tool traverse direction and thickness direction. Thus, no combination of possible shear plane and shear direction aligns with the stir zone / TMAZ interface.

5. Advancing Shoulder

The advancing shoulder demonstrates characteristics similar to those of the retreating shoulder. Although displaying a more distinct delineation between microstructural regions in optical microscopy results, the advancing shoulder region exhibits the same formation of martensitic beta well into base metal and an extended TMAZ region. (Figure 3.5)

The shear texture developed at the advancing shoulder, like the retreating shoulder, begins to deviate significantly from the C-type shear texture observed under the tool (Figure 4.7b). None of the possible slip directions of the face centered cubic lattice aligns with the interface and one slip direction is aligned almost perpendicular to the TMAZ / stir interface.

Altogether, these observations for the 516 sample reveal a shear direction alignment in the direction of tool advance along the bottom of the stir zone / TMAZ interface (retreating corner to advancing corner). Elsewhere, however, the lattice orientation is inconsistent and varies from point to point. At the shoulder locations, both shear/slip direction and lattice orientation appear to be random.

C. FSP 520

The 520 sample condition was processed with a tool rotation rate of 1000 rpm and a traversing speed of 8 ipm. The same tool used for both the 516 and 520 samples. At the level of optical microscopy there is little difference between the two FSP conditions. Although processed at a higher rotation rate, which would lead to more severe adiabatic heating, the stir zone of the 520 does not exhibit an appreciable increase in size over the 516; this may reflect the higher traversing rate which would reduce the effective heat

input in much the same manner as an increase in welding heat source speed decreases welding heat input. The most note-worthy difference is slightly larger region involving a "flowing" pattern on the retreating side of the 520 sample. OIM scans were completed in the same manner as for the 516 sample. The only differences were in the pattern of multiple scans at the retreating side and advancing side corners, as explained in experimental procedure chapter. The following observations were made of the 520 sample.

1. Retreating Shoulder

Examination of the retreating shoulder region of the FSP 520 sample reveals optical and OIM results analogous to the FSP 516 sample. This region of the sample is characterized by an indistinct transition from stir zone into TMAZ (Figure 3.5b). Figure 4.8c illustrates a shear texture that is significantly rotated away from the C-type component in the sample axis system, although a {001}<110> combination can be identified that is nearly tangent to the stir zone / TMAZ interface.

2. Retreating Corner

Similar results to those observed in the 516 sample were again observed. The retreating side corner displays a less distinct transition from stir zone into the TMAZ. The shear texture developed at this location is similar to the C-type shear but it does not coincide as well with the sample axes as it did in the 516 sample. The shear texture developed at the retreating corner in the 520 sample does not exhibit a tendency for the shear direction to align in the direction of tool advance. (Figure 4.9b) However a {001}<110> combination can be identified that is nearly tangent to the stir zone / TMAZ interface in this region. For this orientation a <110> is aligned with this interface as well as with the direction of tool advance.

3. Sample Center

The transition between stir zone and TMAZ is now very distinct in the 520 sample, as was the case with the 516 sample. The texture developed at the sample center

exhibits attributes similar to the C-type shear texture although it is less well aligned with the interface when comparison is made to the 516 sample. Nevertheless, there is a {011}<110> combination that is nearly aligned with the interface in this location. (Figure 4.10b)

4. Advancing Corner

The advancing corner location displays a very sharp transition from stir zone into TMAZ (Figure 4.11a). In this sample there is no {011}<110> combination that is nearly aligned with the interface at this location. Rather, the most prominent orientation in the TMAZ is a <111> aligned with the direction of tool advance, which is contrary to FSP 516 at this location (Figure 4.6b).

5. Advancing Shoulder

The advancing shoulder of the FSP 520 exhibits a C-type shear texture in the TMAZ. This may be seen in Figure 4.12b. Again, there is no {001}<110> combination that aligns with the stir zone / TMAZ interface although a <110> is aligned almost perpendicular to the sample surface.

Figure 4.14 displays summaries of the lattice orientations in the TMAZ region for the results obtained in this study. In all cases single orientations were observed that correspond to the C-type shear texture component. For both processing conditions, the shear plane / shear direction associated with the C component align with the stir zone / TMAZ interface only at locations immediately below the tool. Elsewhere, the lattice orientation does not exhibit such an alignment. It is possible that this reflects a complex interaction between the local lattice orientations of the grains in the as-cast material and the deformation and heating associated with FSP.

It is important to note that, due to crystal symmetry, it is not possible to distinguish whether the local shear direction, which is assume to correspond to a <110>, is in the direction of tool advance or perpendicular to the direction of tool advance when the C component aligns with the sample axes. It may be assumed, due to the nature of the process, that the slip directions are in the direction of tool advance for FSP 516; and

previous studies support the findings for FSP 520. The opposing directions / orientations, however, can not be ruled out.

The differences in the FSP 516 and FSP 520 samples suggests that there may be threshold in which rotation rate dominates over translation speed in the development of shear textures in NAB. This is supported by work done by Cuevas [Ref. 7] on FSP 379 processed at a rotation rate of 800 rpm and a translation speed of 1 ipm. Cuevas' work reveals shear direction alignments similar to FSP 516 in which the shear direction aligns in the direction of tool advance.

D. THEORY OF TEXTURE DEVELOPMENT

In discussion the results thus far, it has been implied that the state of strain in the TMAZ is approximately one of shear due to tool rotation. In this, the plane of shear would be tangent to the stir zone / TMAZ interface while the shear direction would lie in this same plane and tend to align with the direction of tool surface motion. The variations of lattice orientation observed in the data of this work are not entirely consistent with this supposition. Firstly, it is clear that the stir zone / TMAZ interface is the demarcation line between material that has experienced recrystallization leading to a very fine grain size. The presence of particles has resulted in a nearly random texture in the stir zone and this persists up to this interface. Immediately into the TMAZ a distinct, single component texture becomes apparent. The variation in texture orientation around the periphery of the stir zone suggests a possible alternative explanation for texture development in FSP of this material dominated the displacement of material by the tool. Essentially, it is hypothesized that in the TMAZ deformed material is forced downward (as well as around the tool) as the tool advances. This is a result of the downward pressure exerted on the tool to keep it in place as well as tool translation. As the tool passes a given area the deformed material relaxes, or rebounds, from the downward pressure giving rise to the nearly vertical/normal shear orientations often observed in this research. [Ref 32& Figure 4.13] According to this, the stirred material then represents a mass of metal which "plows" its way across the surface and that tool rotation may have less of an effect on shear at the stir zone / TMAZ interface. Under this consideration, tool rotation serves

mainly to heat and soften the material mass, thereby allowing tool translation and the plowing effect to occur.

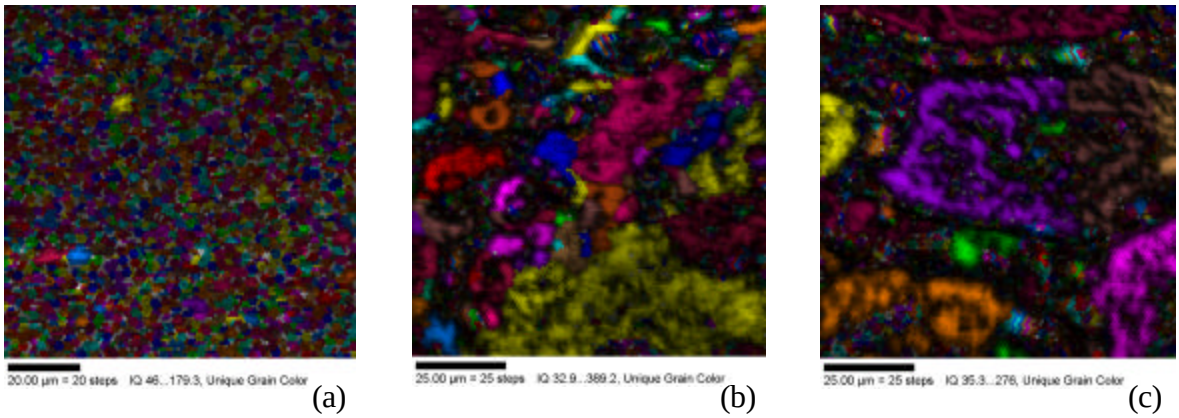

Figure 4.1: OIM images showing change in grain size from (a) stir zone to (b) TMAZ to (c) base metal.

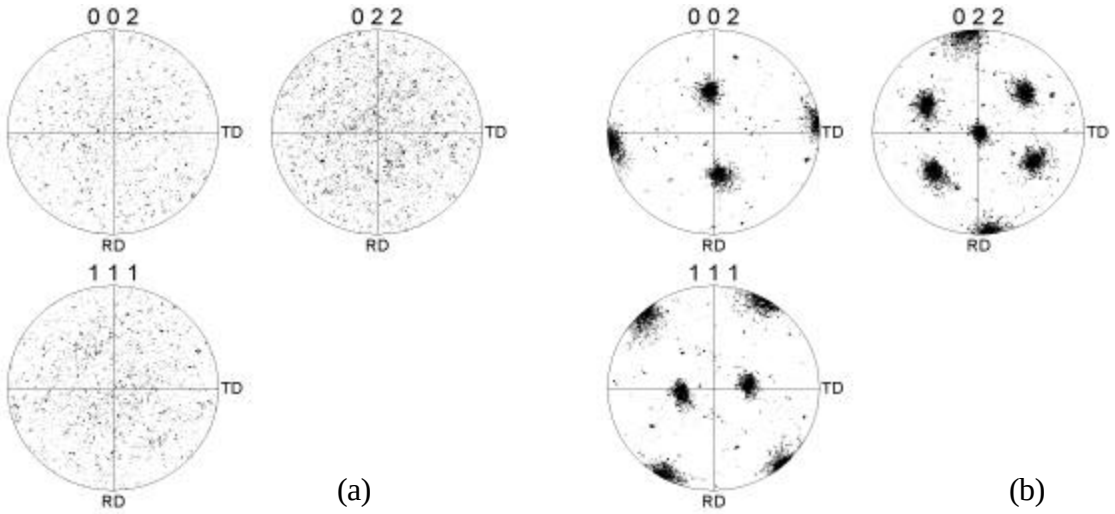

Figure 4.2: Representative a) random orientation and b) C-type shear texture for {002}, {022} and {111} pole figures. Each grain is given a position on the figure. Random orientations are characterized by a random distribution of points (a), while a concentration of grains at preferred locations characterizes texture (b).

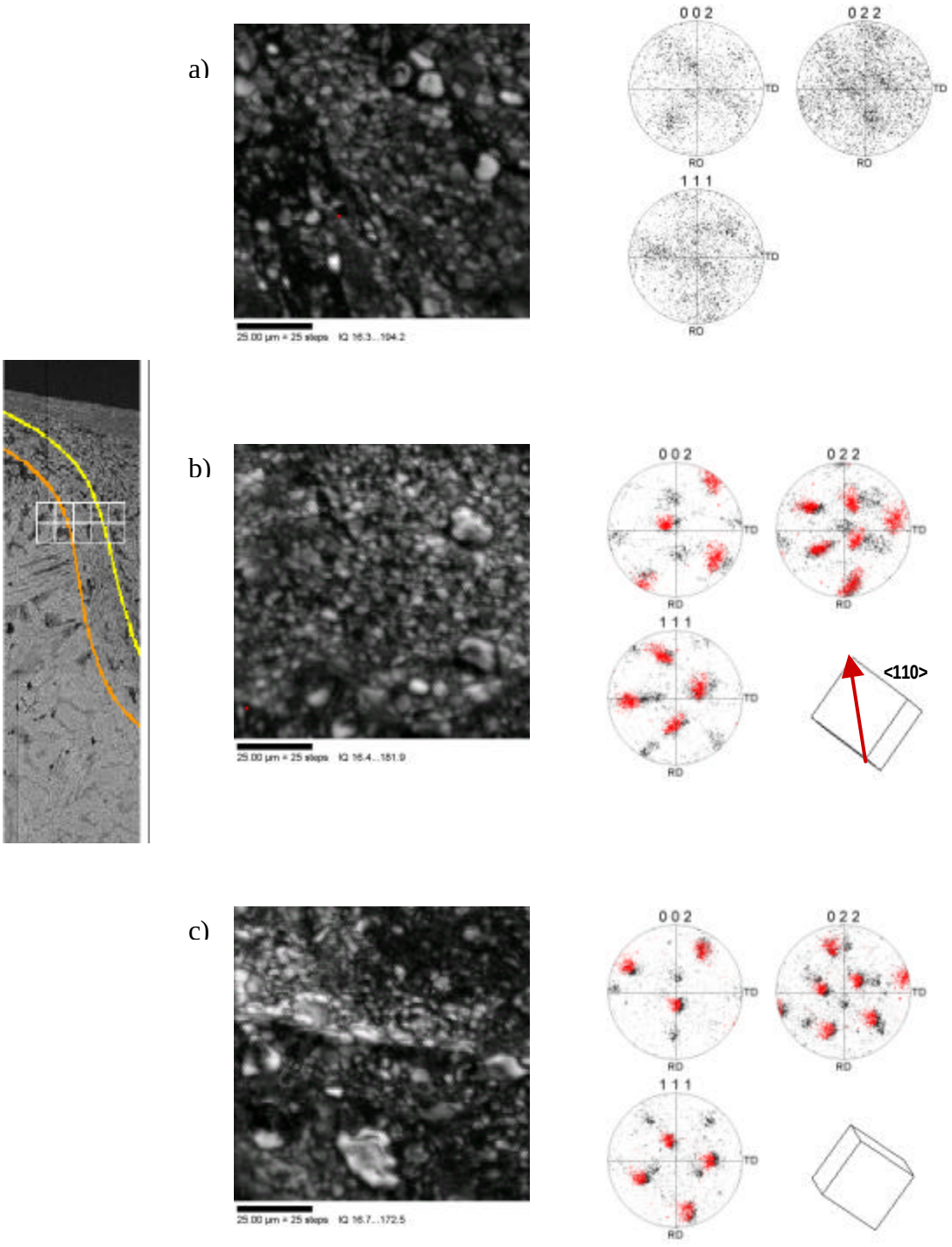

Figure 4.3: Scans of FSP Retreating Shoulder. Scans were completed from the stir zone a) through the TMAZ b) into base metal c). Scans at the shoulders show an extended TMAZ region c). All subsequent figures follow the same format. For all figures (4.3-4.13) red arrows indicate shear directions.

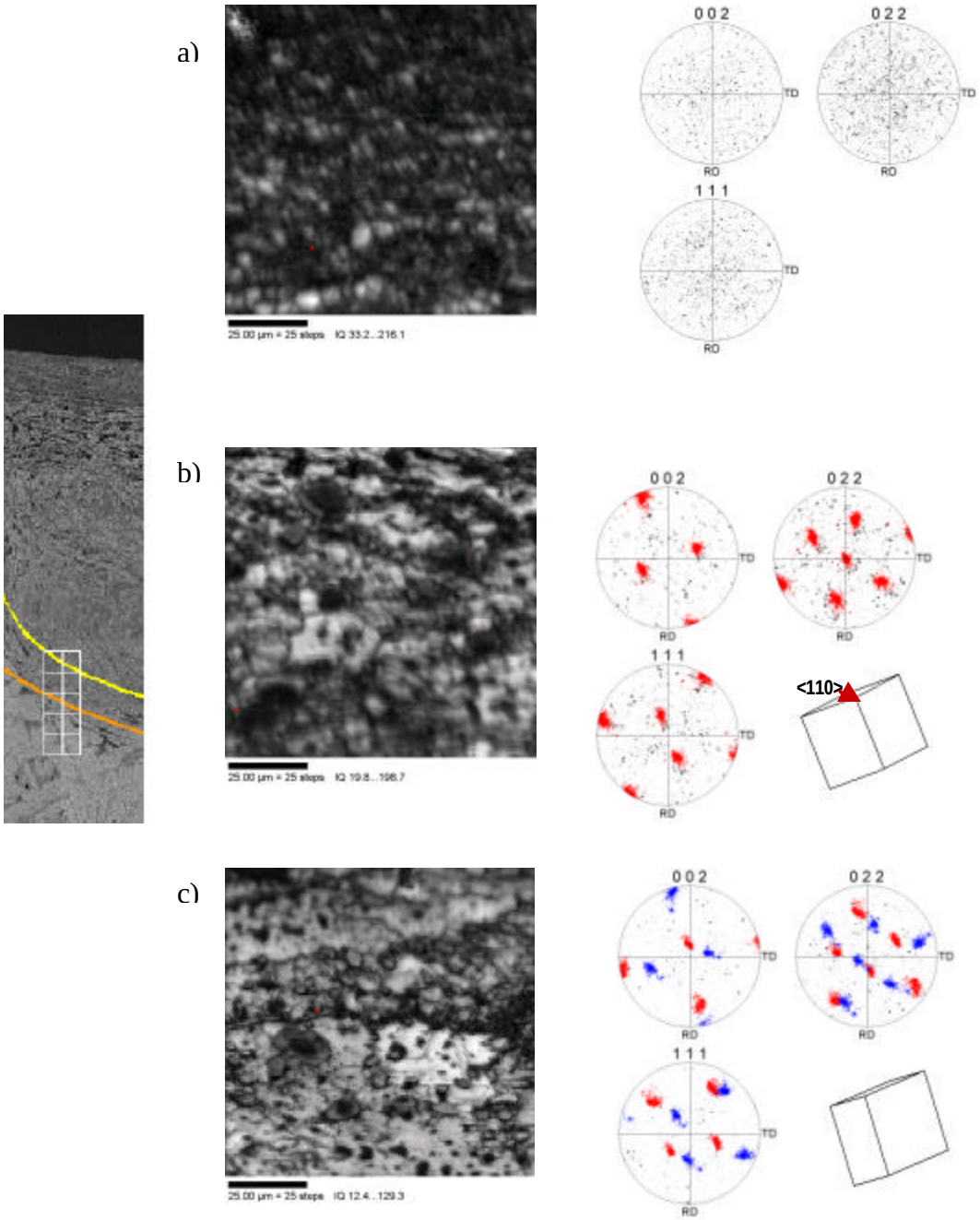

Figure 4.4: Retreating corner scans of FSP 516. Stir zone a), TMAZ b), Base metal c). Base metal is often characterized by the presence of two or more crystallographic orientations.

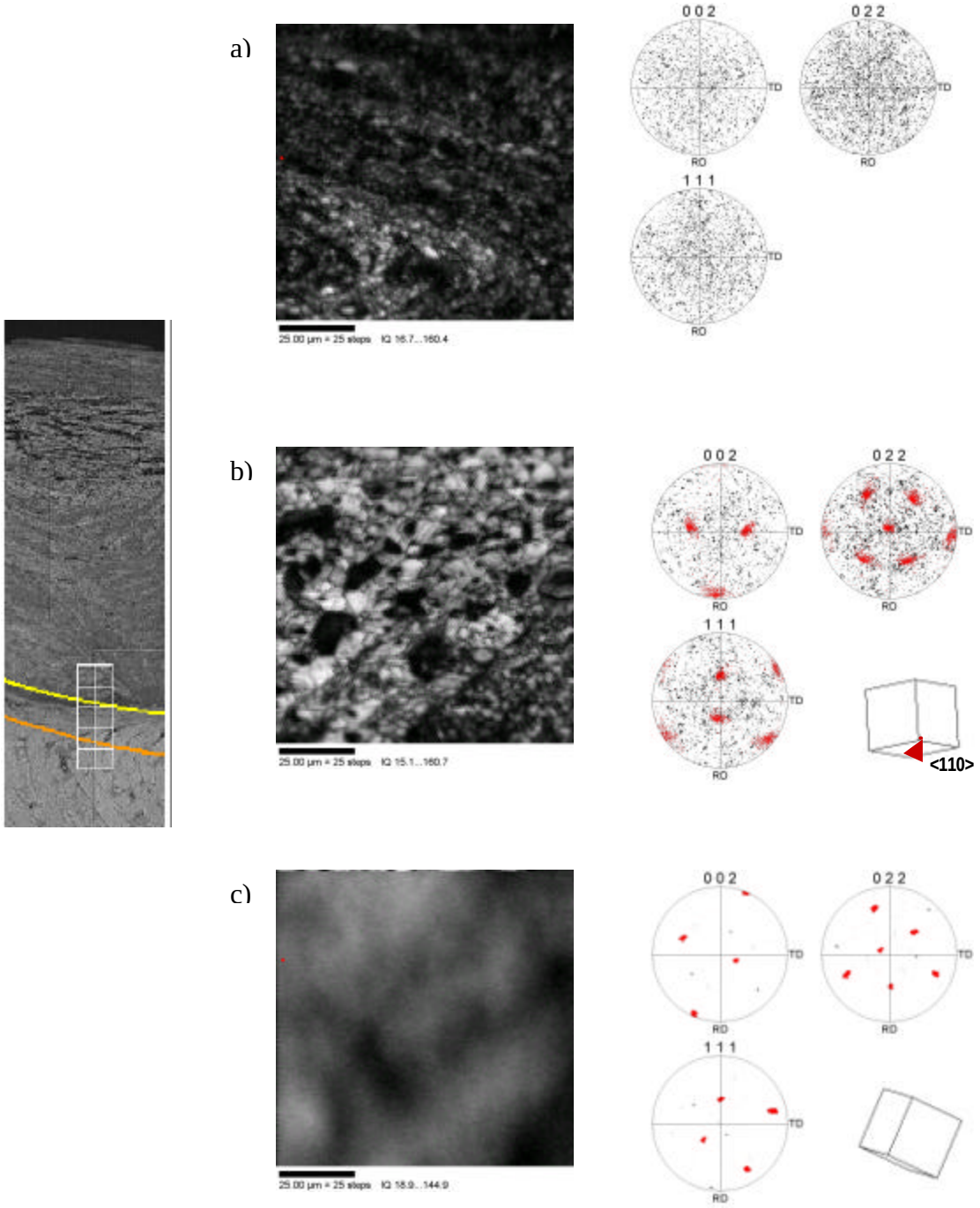

Figure 4.5: Center scans of FSP 516. Stir zone a), TMAZ b) and Base metal c).

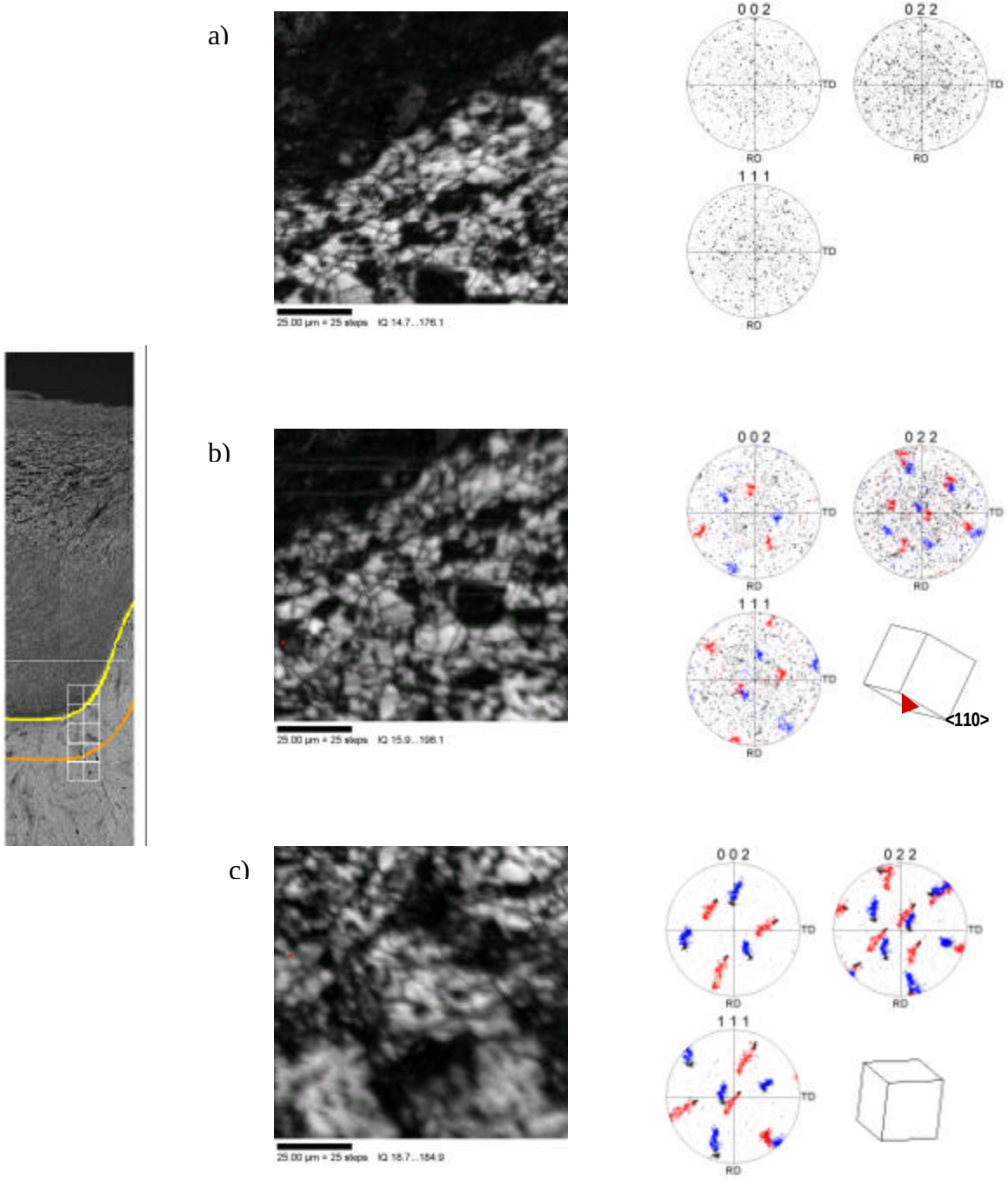

Figure 4.6: Advancing Corner scan of FSP 516. Stir zone a), TMAZ b), Base metal c).

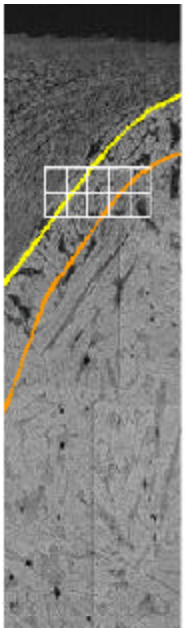

a)

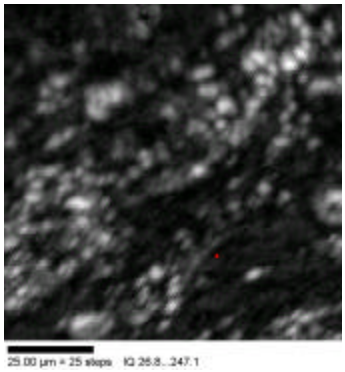

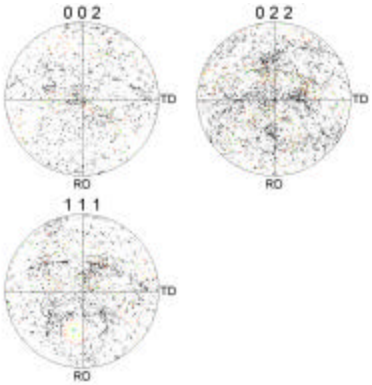

b)

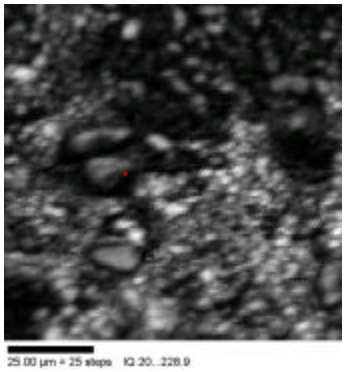

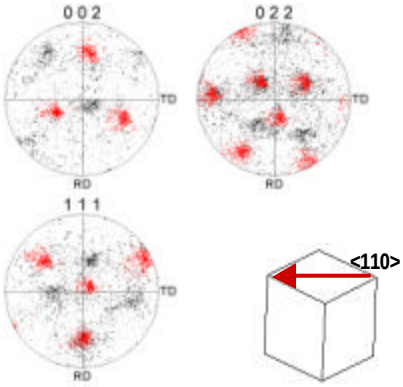

c)

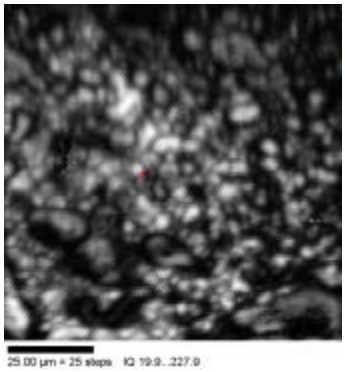

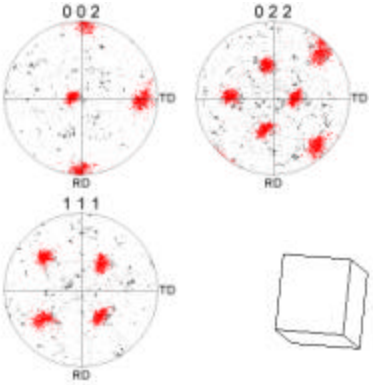

Figure 4.7: Advancing shoulder Scan of FSP 516. Stir zone a), TMAZ b), Extended TMAZ/Base metal c).

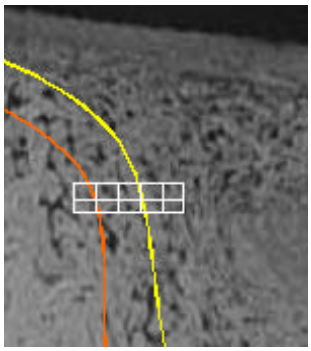

a)

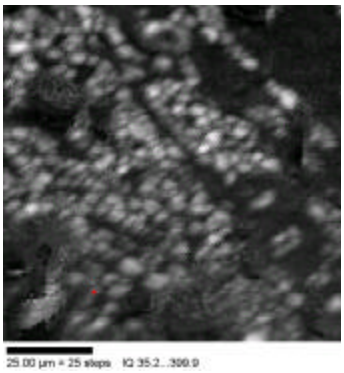

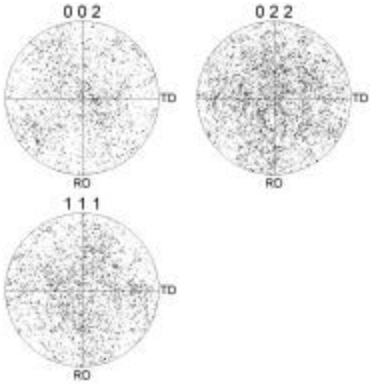

b)

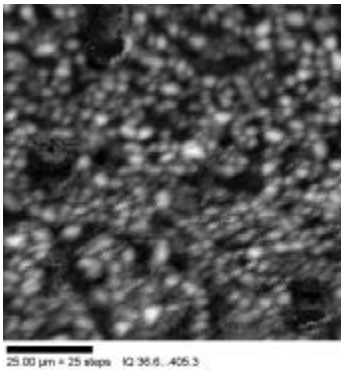

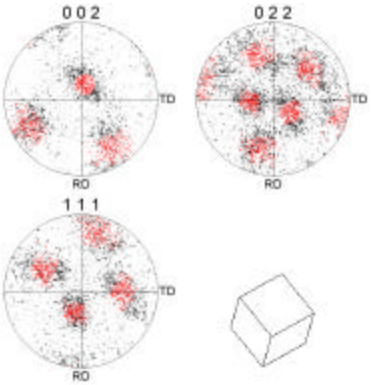

c)

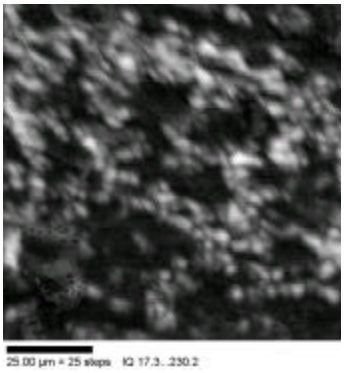

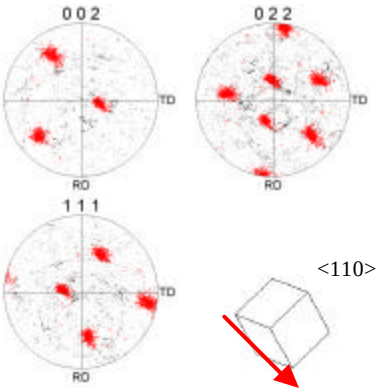

Figure 4.8: Retreating Shoulder scans of FSP 520. Stir zone a), TMAZ b), Extended TMAZ/Base metal c).

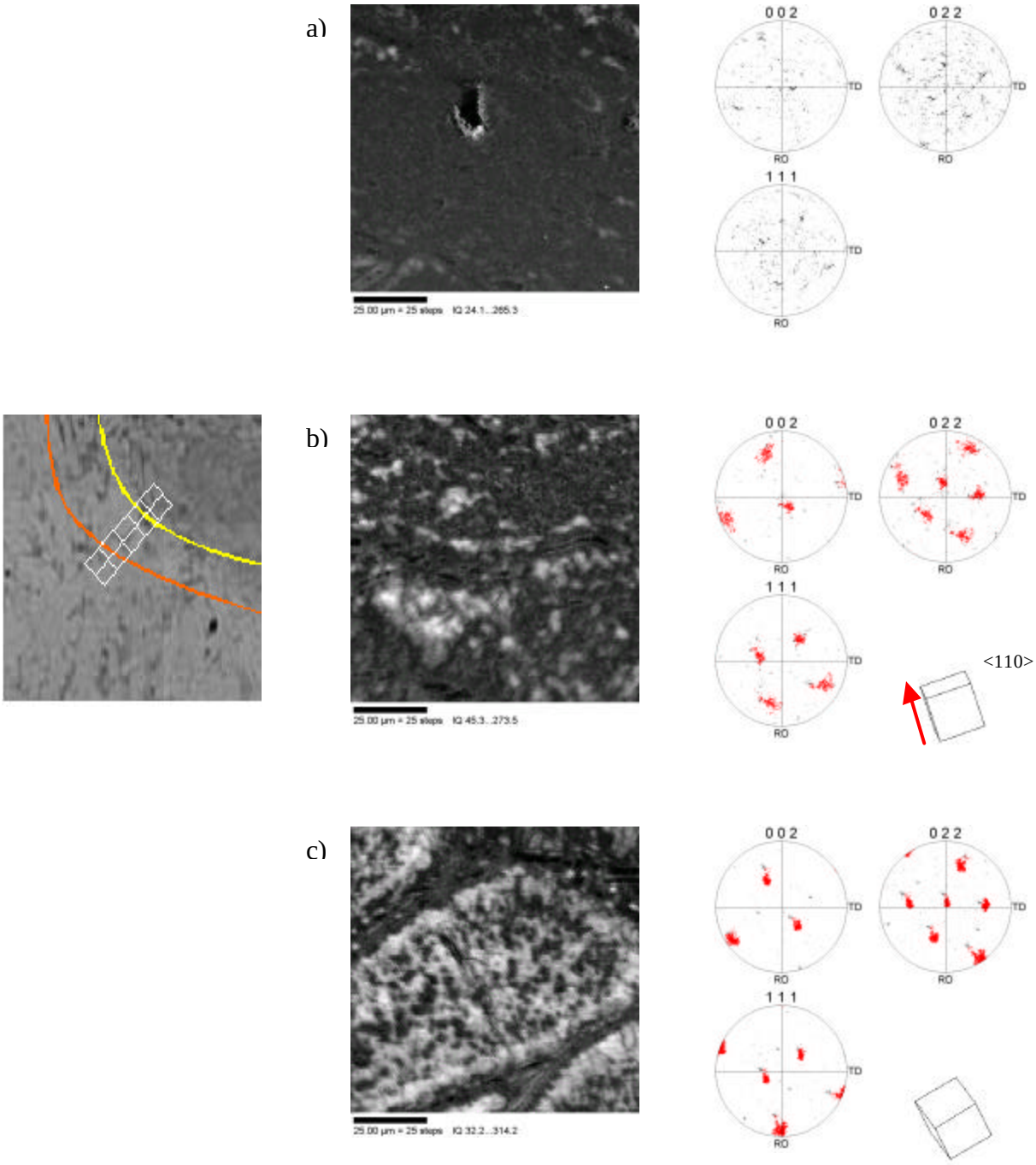

Figure 4.9: Retreating Corner scans of FSP 520. Stir zone a), TMAZ b), Base metal c).

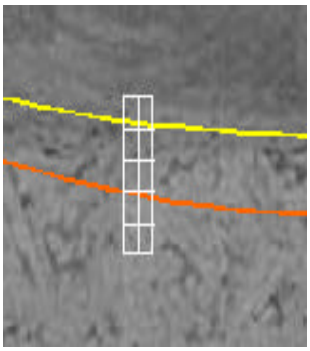

a)

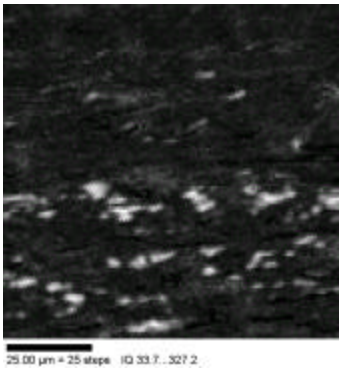

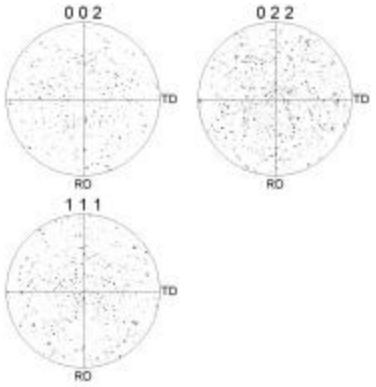

b)

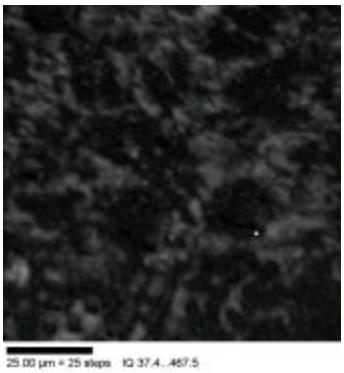

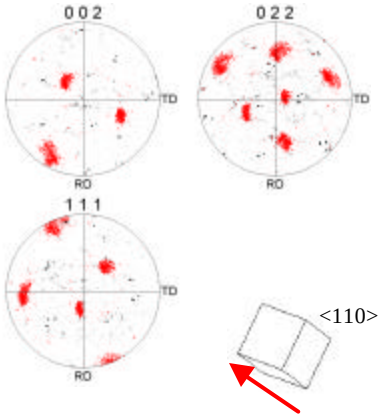

c)

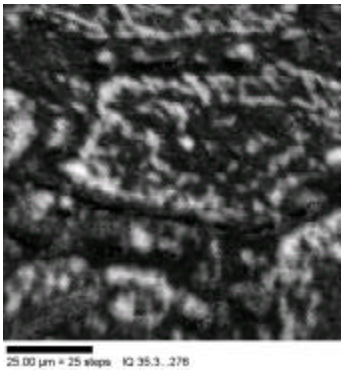

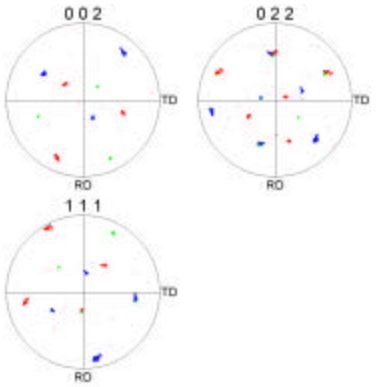

Figure 4.10: Center Scans of FSP 520. Stir zone a), TMAZ b), Base metal c). Notice multiple orientations in base metal.

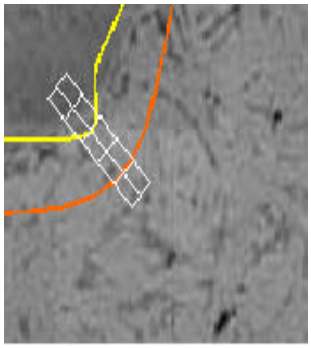

a)

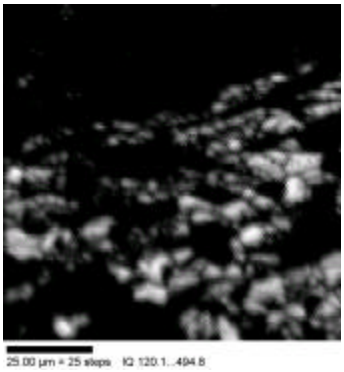

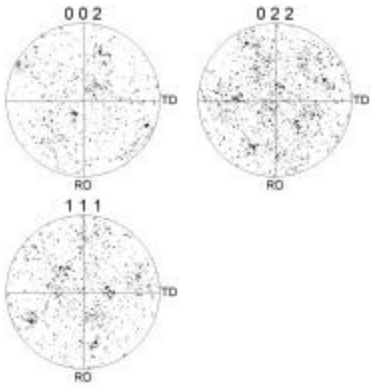

b)

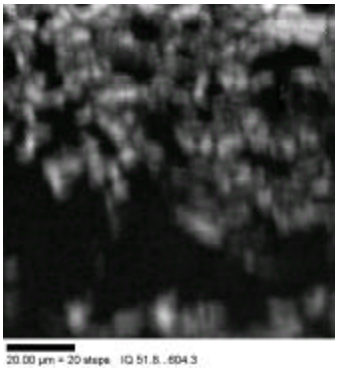

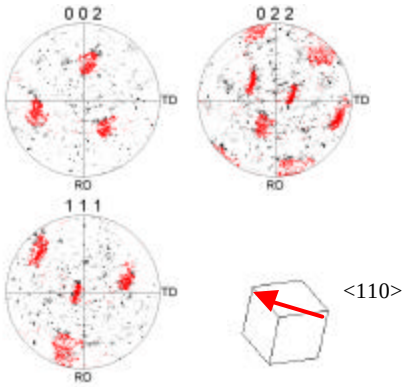

c)

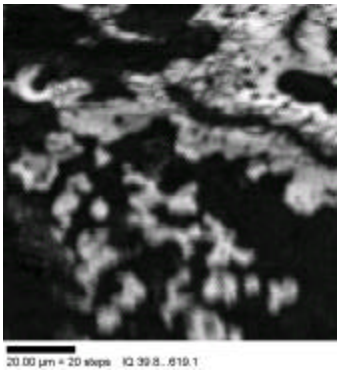

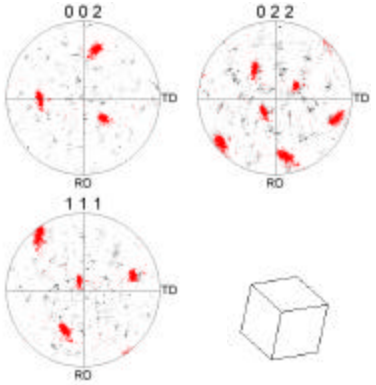

Figure 4.11: Advancing Corner scans of FSP 520. Stir zone a), TMAZ b), Base metal c).

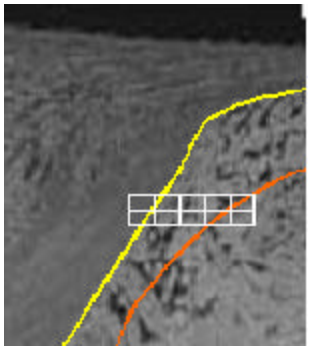

a)

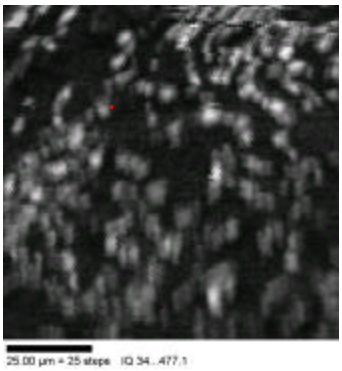

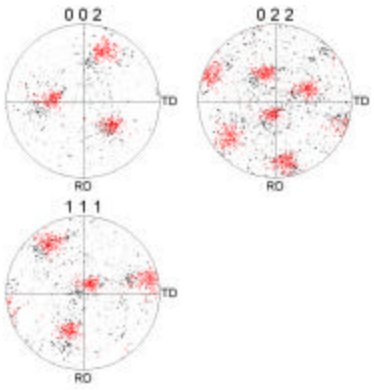

b)

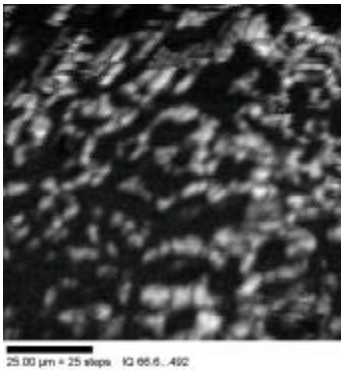

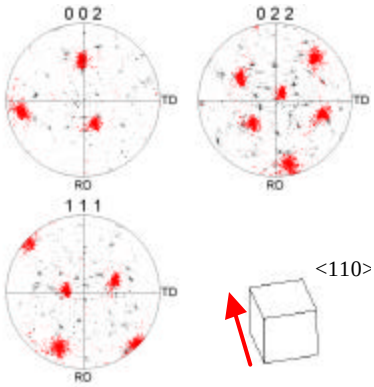

c)

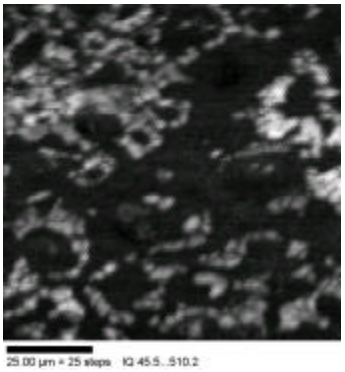

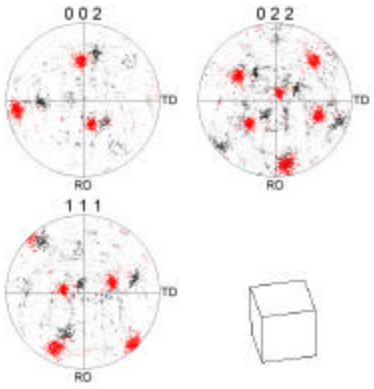

Figure 4.12: Advancing Shoulder scans of FSP 520. Stir zone a), TMAZ b), Extended TMAZ/ Base metal c).

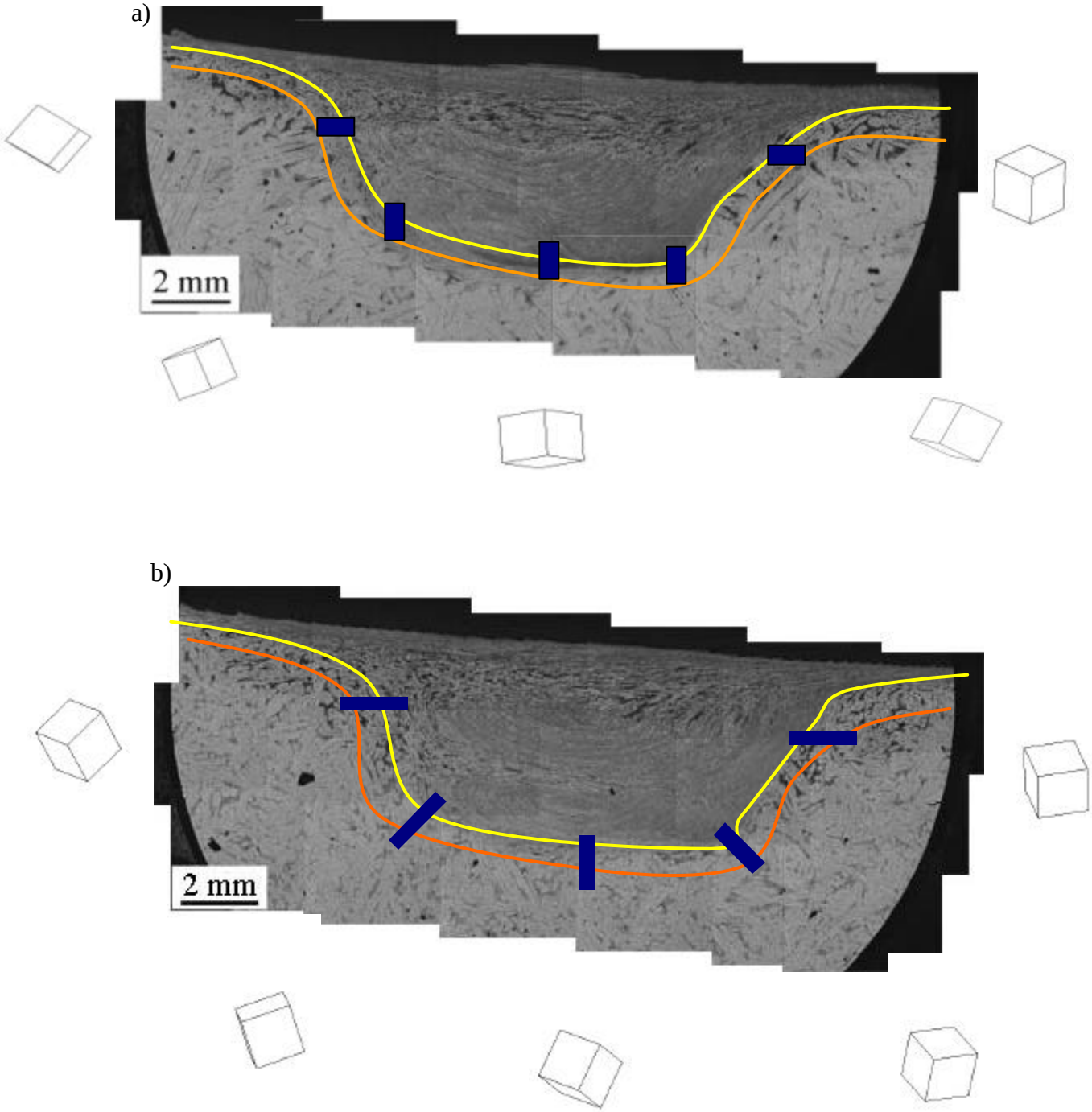

Figure 4.13: Lattice orientations for FSP 516 a) and FSP 520 b).

THIS PAGE INTENTIONALLY LEFT BLANK

V. SUMMARY AND CONCLUSIONS

A. SUMMARY AND CONCLUSIONS

The thermo-mechanically affected zone of friction stir processed NAB represents an area experiencing severe plastic deformation coupled with heating effects. It is characterized by the presence of shear textures and moderately (10 μm) sized deformed grains. The following conclusions were drawn regarding shear textures in the TMAZ of friction stir processed NAB.

1. 516 Sample

(1) OIM is useful in determination and analysis of shear textures in highly deformed materials.

(2) Single component textures, often of the C-type ({001}<110>), were generally present in the lower region of the TMAZ from the lower retreating side corner to the lower advancing side corner. In these regions the shear or slip direction <110> was approximately aligned in the direction of tool advance. Local lattice orientations varied around this orientation.

(3) At the retreating and advancing shoulders the shear texture deviated from the C-type component. At these locations, the shear direction varied with no apparent preferred orientation.

(4) Apparent shear alignment along bottom of the stir zone/ TMAZ interface may be consistent with tool rotation in the TMAZ for this condition.

(5) Shear textures and behaviors in NAB are contrary to those of other FSW and FSP'd materials such as Al and Mg, wherein shear planes consistently align tangent to the TMAZ or tool interface.

2. 520 Sample

(1) Observed {001}<110> orientations different from those seen in the 516 sample. FSP 520 exhibits characteristics that may be more congruent with effects seen in Mg and Al alloys, at least under the tool.

(2) Increases in both rotation rate and traversing speed did not significantly alter the size or appearance of stir zone or TMAZ.

(3) Processing conditions of 520, as well as previous work, suggest that the translation speed vs. rotation rate relationship requires a systematic approach to studying the effects of tool rotation and tool translation. Increased rotation rates may alter the extent of vertical flow of material accounting for tangent shear orientations.

Overall, this study concludes that a full interpretation of shear textures on FSP NAB cannot be accomplished through observation alone. Modeling coupled with experimentation may provide the information necessary to determine the local stress states in the material, leading to increased understanding of the process.

B. RECOMMENDATIONS FOR FURTHER STUDY

It is recommended that further investigation of the dynamics governing the advancing and retreating sides be completed. This will aid in the overall understanding of the friction stir process. In addition, a more systematic study on the effects of tool translation speed vs. rotation rate is needed. If accomplished, a hypothesis on which mechanisms, or combination of mechanisms, are dominant in FSP can be made. Ultimately, a determination of why**,** versus what, observed shear orientations and textures develop in NAB is needed; and represents the depth of understanding required before undertaking large-scale employment of FSP.

LIST OF REFERENCES

1. Duma, J.A., "Heat Treatments For Optimizing Mechanical and Corrosion Resisting Properties of Nickel-Aluminum Bronzes," *Naval Engineers Journal*, v. 87, p. 45-64,1975.

2. Metals Handbook, 9th Ed., v. 2, Properties & Selections: Nonferrous Alloys and Pure Metals.

3. Military Specifications For Bronze, Nickel-Aluminum (UNSC95800), Castings For Seawater Service (MIL-B-24480A), 20 June 1985.

4. American Society for Testing and Materials (ASTM) B148 -- 93a, Standard Specification for Aluminum-Bronze Sand Castings.

5. Sahoo, M., "Structure and Mechanical Properties of Slow-Cooled Nickel-Aluminum Bronze Alloy C95800," *AFS Trans*, v. 90, p. 913-926, 1982.

6. Culpan, E.A. and Rose, G., "Corrosion Behaviour of Cast Nickel Aluminium Bronze in Sea Water," *British Corrosion Journal*, v. 14, p. 160-166, 1979.

7. A.M. Cuevas, Master's Thesis, "Microstructure Characterization of Friction-Stir Processed Nickel-Aluminum Bronze through Orientation Imaging Microscopy," Naval Postgraduate School, Monterey, CA, 2002.

8. W.M. Thomas, E.D. Nicholas, J.C. Needham, M.G. Murch, P. Templesmith and C.J. Dawes, "Friction Stir Butt Welding," G.B. Patent Application No. 9125978.8, Dec. 1991; U.S. Patent No. 5460317, October 1995.

9. Mishra, R.S. and Mahoney, M.W., "Friction Stir Processing: A New Grain Refinement Technique to Achieve High Strain Rate Superplasticity in Commercial Alloys," *Materials Science Forum*, v. 357-359, p. 507-514, 2001.

10. P.B. Berbon, W.H. Bingel, R.S. Mishra, C.C. Bampton and M.W. Mahoney, "Friction Stir Processing: A Tool to Homogenize Nanocomposite Aluminum Alloys," *Scripta Materialia*, v. 44, p. 61-66, 2001.

11. R.S. Mishra, M.W. Mahoney, S.X. McFadden, N.A. Mara and A.K. Mukherjee, "High Strain Rate Superplasticity In A Friction Stir Processed 7075 Al Alloy," *Scripta Materialia*, v. 42, p. 163-168, 2000.

12. Weston, G.M., "Survey of Nickel-Aluminium-Bronze Casting Alloys on Marine Applications," Australia Dept. of Defence Report, DSTO MRL, Melbourne, Victoria, MRL-R-807, 1981.

13. Weill-Couly, P. and Arnaud D., "Influence De La Composition Et De La Structure Des Cupro-Aluminiums Sur Leur Comportment En Service," *Fonderie*, no. 322, p. 123-135, 1973.

14. Culpan, E.A. and Rose, G., "Microstructural Characterization Of Cast Nickel Aluminium Bronze," *Journal of Materials Science*, v. 13, p. 1647-1657, 1978.

15. F. Hasan, A. Jahanafrooz, G.W. Lorimer and N. Ridley,"The Morphology, Crystallography, and Chemistry of Phases in As-Cast Nickel-Aluminum Bronze," *Met. Trans A*, v. 13a, p.1337-1345, 1982.

16. A. Jahanafrooz, F. Hasan, G.W. Lorimer and N. Ridley, "Microstructural Development in Complex Nickel-Aluminum Bronze," *Met. Trans A*, v. 14a, p. 1951-1956, 1983.

17. D.E. Bell, Master's Thesis, "Microstructural Development and Corrosion Resistance of Laser-Welded Nickel-Aluminum Bronze," Pennsylvania State University, PA, 1994.

18. Private communications, M.W. Mahoney, Rockwell Science Center, Thousand Oaks, CA, November 2002.

19. D.P. Field, T.W. Nelson, Y. Hovanski and K.V. Jata, "Heterogeneity of Crystallographic Texture in Friction Stir Welds of Aluminum," *Met. And Mat. Trans. A*, v. 32a, p. 2869-2877, 2001.

20. S.H.C. Park, Y.S. Sato, and H. Kokawa, "Basal Plane Texture and Flow Pattern in Friction Stir Weld of Magnesium Alloy," *Met. And Mat. Trans. A*, v. 34a, p. 987-994, 2003.

21. G.R. Canova, U.F. Kocks and J.J. Jonas, "Theory of Torsion Texture Development," *Acta Metall.*, v. 32, p. 211-226, 1984.

22. Private communications, W. A. Nabach, Naval Postgraduate School, Monterey, CA, May 2003.

23. Metals Handbook 10th Ed., 1990.

24. Private communications, A. Askari, Boeing, Inc., April 2003.

25. Private communications, K. Oishi, Naval Postgraduate School, Monterey, CA, May 2003.

26. Private communications, C. Park, Naval Postgraduate School, Monterey, CA, May 2003.

27. Brezina, P, “Heat Treatment of Complex Aluminum Bronzes,” *Int. Met. Rev*., v. 27, n. 2, p. 77-120, 1982.

28. Orientation Imaging Microscopy (OIM) Data Collection User Manual, ver. 1.0, TexSEM Laboratories, Inc., 1998.

29. Orientation Imaging Microscopy (OIM) Analysis, ver. 3.0, TexSEM Laboratories, Inc., 2000.

30. D.L. Swisher, Master’s Thesis, “Production of Ultra-Fine Grains and Evolution of Grain Boundaries During Severe Plastic Deformation of Aluminum and its Alloys,” Naval Postgraduate School, Monterey, CA, 2000.

31. S.D. Terhune, Z. Horita, M. Nemoto, Y. Li, T.G. Langdon and T.R. McNelley, ”The Evolution of Microtexture and Grain Boundary Character during ECA Pressing of Pure Aluminum,” *Intl. Conf. On Recrystallization and Related Phenomena*, p. 515-522, 1999.

32. Private communications, M.W. Mahoney, Rockwell Science Center, Thousand Oaks, CA, June 2003.

THIS PAGE INTENTIONALLY LEFT BLANK

INITIAL DISTRIBUTION LIST

1. Defense Technical Information Center
   Ft. Belvoir, Virginia

2. Dudley Knox Library
   Naval Postgraduate School
   Monterey, California

3. Engineering and Technology Curricular Office, Code 34
   Naval Postgraduate School
   Monterey, California

4. Department Chairman, Code ME/Kw
   Naval Postgraduate School
   Monterey, California

5. Professor Terry R. McNelley, Code ME/Mc
   Naval Postgraduate School
   Monterey, California

6. ENS Charles F. Walton, Jr.
   Mission Viejo, California

7. Dr. Leo Christodoulou
   DARPA/DSO
   Arlington, Virginia

8. Murray W. Mahoney
   Rockwell Science Center
   Thousand Oaks, California

9. William Palko
   Naval Surface Warfare Center
   Carderock Division
   West Bethesda, Maryland